# DEVELOPMENT AND CHARACTERIZATION OF LIGHT-WEIGHT ARMOR MATERIALS

**A Thesis Submitted to**
**the Graduate School of Engineering and Sciences of**
**İzmir Institute of Technology**
**in Partial Fulfillment of the Requirements for the Degree of**

**MASTER OF SCIENCE**

**in Materials Science and Engineering Program**

**by**
**Erol ÜNALER**

**July 2005**
**İZMİR**

We approve the thesis of **Erol ÜNALER**

**Date of Signature**

……..
**Assoc. Prof. Dr. Metin TANOĞLU** **25 July 2005**
Supervisor
Department of Mechanical Engineering
İzmir Institute of Technology

……..
**Assoc. Prof. Dr. Mustafa GÜDEN** **25 July 2005**
Co-Supervisor
Department of Mechanical Engineering
İzmir Institute of Technology

……
**Prof. Dr. Muhsin ÇİFTÇİOĞLU** **25 July 2005**
Department of Chemical Engineering
İzmir Institute of Technology

……
**Assoc. Prof. Bülent YARDIMOĞL**U **25 July 2005**
Department of Mechanical Engineering
İzmir Institute of Technology

……
**Asst. Prof. H.Seçil ALTUNDAĞ ARTEM** **25 July 2005**
Department of Mechanical Engineering
İzmir Institute of Technology

……
**Prof. Dr. Muhsin ÇİFTÇİOĞLU** **25 July 2005**
Head of Materials Science and Engineering Program
İzmir Institute of Technology

……
**Assoc.Prof.Dr. Semahat ÖZDEMİR**
Head of the Graduate School

# ABSTRACT

In this study, E-glass/unsaturated polyester composite laminates using woven and non-crimp stitched fabrics and isophtalic and orthophthalic polyester resin were fabricated using RTM (Resin Transfer Molding) technique. In addition to composite laminates, multilayered sandwich laminates using aluminum (Al) plates and alumina ($Al_2O_3$) tiles were manufactured to improve the ballistic resistance of the composite structure. An experimental investigation was carried out to determine the mechanical and ballistic performance of E-glass/unsaturated polyester composite laminates with and without aluminum and alumina tiles. The mechanical properties of the composite laminates made with $0^o/90^o$ woven fabrics and $0^o/90^o$ and $0^o/-45^o/+45^o/90^o$ non-crimp stitched fabrics and two resin systems were measured for comparison of fabric and resin types. The flexural strength and modulus, compressive strength and modulus through ply-lay up and in plane loading directions, mode I interlaminar fracture toughness and apparent interlaminar shear strength of the composites were measured to evaluate the effects of the fiber architecture on the mechanical properties of the composites. It was found that in general the mechanical properties of the composites made with $0^o/90^o$ woven fabrics are higher than those of the composites made with multiaxial non-crimp stitched fabrics. Moreover, the composite plates with and without aluminum plates and alumina tiles were subjected to ballistic impact by AP (armor piercing), FSP (fragment simulating projectile) and ball (B) type projectiles with initial velocities in the range of 420-1173 m/s. The ballistic test results exhibit that the polymer composites have ballistic resistance against 7.62 mm fragment simulating projectiles (FSP) up to 1001 m/s projectile velocities. However, the composites without any support layer are not sufficient to stop AP projectiles. The sandwich panels containing ceramic tiles subjected to the ballistic impact by AP and FSP projectiles exhibited only partial penetrations at all the velocities applied within the study (446-1020 m/s with AP and 435-1173 m/s with FSP). The extensions of damages in the composites were evaluated after impact. It is concluded that the multilayered composite structures have capacity against the ballistic threats and potential to be used as lightweight armor materials.

# ÖZET

Bu çalışmada, E-cam/doymamış poliester kompozit laminalar örgü ve kıvrımsız dikişli cam elyaf kumaş ve isophtalic and orthophthalic poliester reçinelerden RTM (reçine transfer kalıplama) tekniği kullanılarak üretilmiştir. Kompozit laminalara ek olarak, kompozit yapının balistik dayanımını artırmak amacıyla aluminyum plakalar ve alumina tabakalar ilave edilmiştir. Aluminyum (Al) plakaları ve alumina ($Al_2O_3$) tabakalar kullanılarak çok tabakalı sandiviç laminalar üretilmiştir. Aluminyum ve alumina içeren ve içermeyen E-cam/doymamış polyester kompozit laminaların mekanik ve balistik performansını belirlemek amacıyla deneysel çalışma sürdürülmüştür. $0^o/90^o$ örgü, $0^o/90^o$ ve $0^o/-45^o/+45^o/90^o$ kıvrımsız dikişli kumaştan ve iki farklı reçine kullanılarak üretilen kompozit laminaların mekanik özellikleri fiber kumaş ve reçine tipinin etkilerini karşılaştırmak için ölçülmüştür. Kompozitlerin eğme mukavemeti ve modülü, tabakalanma yönünde ve tabakalanma yönüne dik yönde basma mukavemeti ve modülü, mod I lamilar arası kırlma tokluğu , laminalar arası akama mukavemeti değerleri fiber kumaş yapısının mekanik özellikler üzerindeki etkisi incelemek üzere ölçülmüştür.. Genel olarak, örgü kumaş ile yapılan kompozit plakaların kıvrımsız dikişli kumaş içeren yapılara göre daha iyi mekanik özelliklere sahip olduğu gözlemlenmiştir. Ayrıca, kompozit plakalar; 7.62 mm zırh delici (AP), fragment simülasyon mermi (FSP) ve ball (B) mermi ile 420-1173 m/s hızları arasında balistik teste tabi tutulmuştur. Balistik test sonuçları polimer kompozitlerin 7.62 mm fragment simulating projectiles (FSP) e karşı 1001 m/s mermi hızlarına kadar dayanımlı olduğunu göstermiştir. Ancak, bu kompozitler herhangi bir destek tabakasına sahip olmadan zırh delici (AP) mermilerini durdurmada yetersizdir. Seramik tabaka içeren sandvic paneller ise AP ve FSP mermilerinin darbesi karşısında bu çalışmada uygulanan tüm hız aralıklarında (446-1020 m/s AP için 435-1173 m/s FSP için) sadece kısmi penetrasyon göstermiştir. Çarpma sonrasında kompozitlerin hasar yüzeyleri incelenmiştir. Sonuç olarak çok tabakalı kompozit yapıların balistik tehditlere karşı kapasitesinin olduğu ve hafif zırh malzemesi olarak kullanılabileceği gözlemlenmiştir.

# TABLE OF CONTENTS

# LIST OF FIGURES

# LIST OF TABLES

# CHAPTER 1

## INTRODUCTION

Fiber-reinforced composite materials have become important engineering materials used such as marine bodies, aircraft structures and light-weight armor for ballistic protection in military applications. This is due to their outstanding mechanical properties, flexibility in design capabilities, ease of fabrication and good corrosion, wear and impact resistant (Wang *et al.* 1997, Horsfall 2000). There have been a number of experimental investigations on the perforation behaviour of a wide variety of polymer composite laminates made of thermoset resins reinforced with glass, aramid, carbon or polyethylene fabrics (Larsson *et al.* 2002, Ulven *et al.* 2003, Morye 2000).

Weight reduction of the armor system brings the mobility and transportability. Traditional single component armor systems such as steel, aluminum, titanium and ceramic are not the most effective one against the ballistic threat. Besides, the integral armor is the most effective armor system that contains a number of layers each has special purposes. Integral composite armor system includes a strong, brittle, hard faced material which blunt and wear down the projectile. The hard faced materials may be selected as aluminum nitrate $(Al_2NO_3)_3$, aluminum oxide $(Al_2O_3)$, boron carbide $(B_4C)$, and silicon carbide (SiC). Also, the integral armor structure has a ductile backing plate, which can be steel, aluminum or glass fiber reinforced plastics (GFRP) to absorb the remaining kinetic energy and arrest the projectile and the ceramic fragments. As backing plates, glass fibers (S-2 glass, E-glass) are being employed with epoxy, vinyl ester and polyester resin systems due to their high tensile and compressive strength, good energy absorption properties and relatively lower costs. Also, a layer of an elastomer may be added behind the ceramic tiles for shock attenuation to improve the multi-hit capacity of the armor (Gama *et al.* 2001, Tanoğlu *et al.* 2001, Vaidya *et al.* 2001, Bernetich *et al.* 1998, Mahdi *et al.* 2000, Tanoglu *et al.* 2002).

Resin transfers molding (RTM) and vacuum assisted resin transfer molding (VARTM) techniques have been increasingly utilized to produce high performance polymer composites. RTM has many advantages over other manufacturing processes, including lower labor cost, short cycle time, non-prepregging process, high fiber volume fraction and capability for fabrication of complex structures. In the RTM

process, inadequate fiber wetting, void formation and lower fiber-matrix adhesion lead to reduced mechanical properties and low quality of surface finish (Larsson *et al.* 2002, Ulven *et al.* 2003, Vaidya *et al.* 2001, Bernetich *et al.* 1998, Tanoğlu *et al.* 2002).

One of the objectives of this study is to develop composite armor panels with various fibers and also with additional layers such as ceramic tiles and aluminum plates. Another objective is to utilization of RTM technique to fabricate the mentioned structure. Determination of the mechanical properties and ballistic performance of the composite laminates with and without aluminum and alumina tiles is the final aim.

In the present work, the composite laminates with and without alumina tiles and aluminum plates were manufactured using RTM technique. To determine the mechanical properties, compression, short beam shear, flexural and fracture toughness tests were performed. Also the ballistic test was performed using ball (B), armor piercing (AP), and fragment simulating projectiles (FSPs) to determine the ballistic properties. After the ballistic tests some of the composite armors were sectioned to observe the damaged zones subjected to different impact velocities.

# CHAPTER 2

## ARMOR MATERIALS

### 2.1. Traditional Armor Materials and their Ballistic Limits

Humans throughout recorded history have used various types of materials to protect themselves from injury in combat and other dangerous situations. Armor is generally defined as a defensive covering designed to provide protection from a specific form of attack. Armor has been in use for all recorded history beginning with the hides, leather, bone processing to steel, bronze, ballistic cloth and ceramics. Steel has been traditionally the major armor component. As the projectiles that can perforate an armor are developed, new armor concepts are introduced that can defeat the developed projectiles (Meyers 1994, DEF STAN 05-101). The armor concept can be classified depends on the intended applications as;

1. Body armor (personal armor)
2. Light armor (vehicular and aircraft armor)
3. Heavy armor (tank armor) (Meyers 1994, Candan 2005).

Body armor is intended to protect torso against fragments from high explosive artillery shells, grenades, fragmenting mines, as well as projectiles from small arms. These armors protect against .22 to .30 caliber bullets, with nominal masses of 2.6-10.8 g impacting at the range of velocity of 320-869 m/s (NIJ Standard-01.01.04 ).

In the category of light armor applications, seats in helicopters (protecting against ground fire) and the protection of light vehicles and airplanes can be given as examples. This kind of armor has the capability of protection against the 12.7-25 mm bullets (Candan 2005). A number of different systems have been developed using monolithic metals, ceramic composite armor, polymer composite armor and laminated armor for this purpose. The principal idea is to break the projectile with a very hard surface and then absorb the energy of projectile and or armor fragments by using a soft, ductile backing material (Meyers 1994).

Heavy armor is intended for tanks. Steel has been the principal armor material because of its low cost, ease of fabrication and structural efficiency (Meyers 1994).

The main aim of the armor is maximum protection and mobility of the system. Mobility and speed of the armored vehicle is a key component in its survival in a combat situation and hence the lower the weight, the faster and more maneuverable the vehicle can be for a given power plant. Figure 2.1 shows the historical development of the armor materials with their areal density that is the key on the mobility.

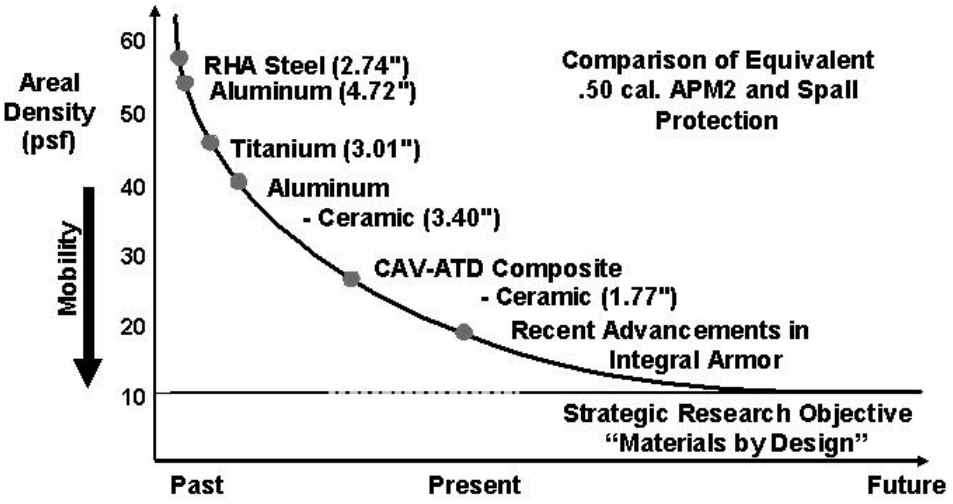


Figure 2.1. The historical development of the armor materials (Source: Tanoğlu *et al.* 2001).

The armor materials can be classified as:

1. Rolled Plate Armor.
2. Cast Armor.
3. Extruded Armor.
4. Forged Armor.
5. Multi-component Armor (Integral armor).
6. Transparent Armor.
7. Fiber Reinforced Plastic Armor.
8. Ceramic Armor.
9. Spall Liners.
10. Armor containing Explosive Material (Reactive armor).
11. Personal Armor Systems (DEF STAN 05-101)

### 2.1.1. Rolled Plate Armor

Rolled homogenous armor is the standard armor material. It is based on the AISI 4340 composition (quenched and tempered steel). There are limitations on the thicknesses in the 7-12 in. range; so can rolled steel. Figure 2.2 represents the ballistic performance for various armor steel (Meyers 1994).

Steel and aluminum alloys are the materials in the rolled plate armor group. Rolled plate armor (for steel) has five different protection classes against the ballistic impacts. The special features and chemical composition of armor steel are tabulated in Tables 2.1 and 2.2, respectively (DEF STAN 95-24/3).

Table 2.1. The mechanical features of rolled plate armor (for steel) (Source: DEF STAN 95-24/3).

| Thickness (mm) | Hardness BHN | UTS (MPa) | Elongation % min | Charpy (J) "V" notch min -40$^{o}$C |
|---|---|---|---|---|
| 3-160 | 262-655 | 895-2400 | 6-15 | 5-42 |

Table 2.2. The chemical compound of rolled plate armor (for steel) (Source: DEF STAN 95-24/3).

| Element | Weight % |
|---|---|
| Sulphur | 0.015 max |
| Phosphorus | 0.015 max |
| Sulphur & Phosphorus Combined | 0.025 max |

The aluminum alloy used as rolled plate armor has the special mechanical properties also. The mechanical properties and the chemical compounds are specified in Tables 2.4 and 2.5, respectively (DEF STAN 95-22).

Table 2.3. The mechanical features of rolled plate armor (for aluminum) (Source: DEF STAN 95-22).

| Thickness (mm) | UTS (MPa) | Elongation % min | 0.2% Proof Stress MPa |
|---|---|---|---|
| 6-120 | 320-460 | 6-8 | 260-390 |

Table 2.4. Chemical compound of rolled plate armor (for aluminum alloy) (Source: DEF STAN 95-22).

| Element | Weight % |
|---|---|
| Zinc | 4.0 - 6.0 |
| Magnesium | 0.7-3.3 |
| Manganese | 0.10-0.70 |
| Copper | 0.10-0.20 |
| Iron | 0.45 max |
| Silicon | 0.35 max |
| Chromium | 0.25 max |
| Titanium | 0.15 max |
| Zirconium | 0.10 - 0.25 |
| Others, each | 0.05 max |
| Others, total | 0.15 max |
| Aluminum (by difference) | Remainder |

### 2.1.2. Cast Armor

Armor quality casting steel's mechanical properties and chemical compositions are shown in Table 2.5 and 2.6, respectively (DEF STAN 95-25). The casting steel can be also used with the combination of rolled plate armor.

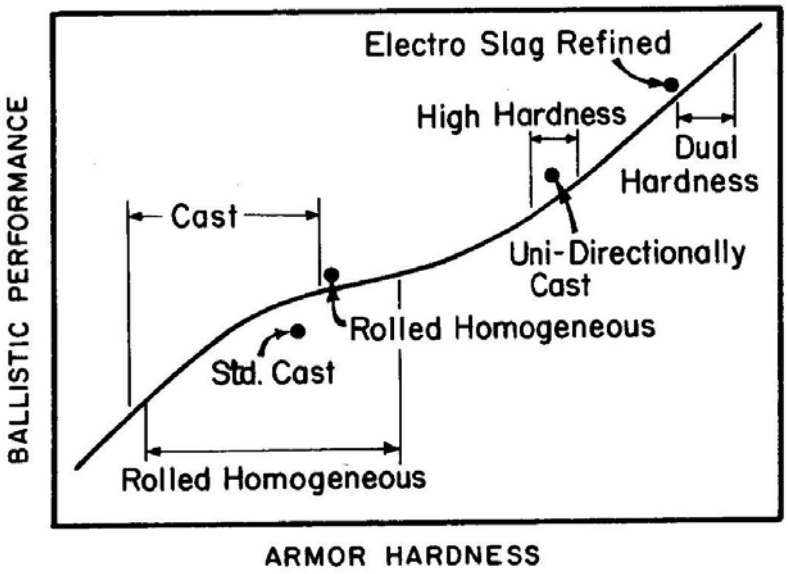


Figure 2.2. Hardness vs. ballistic performance for various armor steel (Source: Meyers 1994).

Table 2.5. The mechanical features of cast armor materials (Source: DEF STAN 95-25).

| Thickness (mm) | Hardness BHN | UTS (MPa) | Elongation % min | Charpy (J) Impact |
|---|---|---|---|---|
| 15-155 | 241-285 | 770 min | 14 min | 40 min |

Table 2.6. The chemical compound of cast armor materials (Source: DEF STAN 95-25).

| Element | Weight (%) |
|---|---|
| Carbon | 0.25 - 0.35 |
| Silicon | 0.20 - 0.60 |
| Manganese | 1.20 - 1.70 |
| Sulphur | 0.020 max |
| Phosphorus | 0.020 max |
| Nickel | 0.50 - 1.00 |
| Chromium | 0.40 - 0.80 |
| Molybdenum | 0.30 - 0.50 |
| Copper | 0.30 max |

### 2.1.3. Extruded and Forged Armor

Extruded steel armor is proofed under Def Stan 95-23 (DEF STAN 95-23). Aluminum armor is covered by Def Stan 95-19 (DEF STAN 95-19). And forged steel armor is proofed under Def Stan 95-23 (DEF STAN 95-23).

### 2.1.4. Ceramic Armor

Ceramics possess two very important qualities that make them ideal candidates for armor materials: high hardness and low density. Ceramic materials can be also used as a matrix material that surrounds the reinforcing material. However; they are generally used in the form of tile shape to be an impactant surface of the composite armor. Ceramic armors are also utilized in two component armor systems which consist of a hard faced material combined with a ductile backing, e.g., aluminum, steel, or glass fiber reinforced plastics (GFRP) (Ranganath *et al.* 1998). Candidate materials depending on the threat and weight constraint for the ceramic tile include aluminum nitrate $(Al_2NO_3)_3$, aluminum oxide $(Al_2O_3)$, boron carbide $(B_4C)$, and silicon carbide (SiC) (Gama *et al.* 1999). The ceramic layer acts to blunt and wear down the projectile and the backing material absorbs the remaining kinetic energy and collects the projectile and the ceramic fragments. As an example, body ceramic armor for low protection is shown in Figure 2.3.

Figure 2.3. Concealable ceramic armor for small arms protection (Source: WEB_1).

Ceramic's low or negligible ductility should not be a factor if they are not used as structural components; thus they are added to the structure. Figure 2.4 shows the relative ballistic efficiencies of several ceramics against impact from a 0.3-in.-diameter

projectile with a conical tip. The penetration of the projectile into the backup plate is measured (Meyers 1994).

A combined numerical and experimental study for the analysis of ceramic/metal composite armor system against 40.7 g steel projectiles has been performed by Lee (Lee *et al.* 2001). It was reported that optimum thickness ratio of the constituents was 2.5 and there were no significant difference between the ballistic performances of two component armor system when the thickness ratio was varied from 1 to 3. Also Navarro investigated the ceramic-faced armors backed by composite plates (Navarro et.al 1993). In that research, the ceramics considered were AD-96 alumina and a mixture of boron nitride and silicon nitride. The backing was a composite plate made of either aramid fibers embedded in a vinylester matrix or polyethylene fibers embedded in a polyethylene resin matrix. It should be said that ceramic-faced armors backed by a metal or composite plate are frequently a weight saving arrangement in armor design.

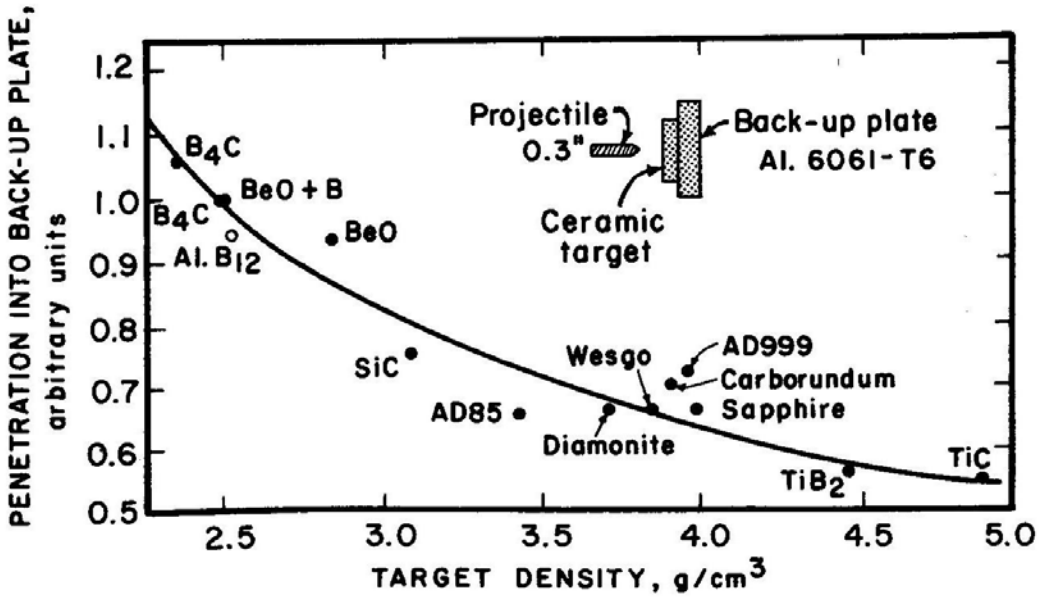


Figure 2.4. Relative ballistic efficiency of various ceramics as a function of their density (Source: Meyers 1994).

## 2.2. Composite Armor

Recent advances in lightweight armor include the development of integral armor systems. It was revealed that the most effective armors are not single component systems based on steel, composite or ceramic materials, however the systems that

combine multi layers of different materials serve well for multifunctionality (Gama 2001, Tanoğlu *et al.* 2001, Vaidya 2001). The sandwich systems usually include an outer ceramic layer that is made of silicon carbide (SiC), boron carbide ($B_4C$), aluminum nitride ($Al_2N_3$) or alumina ($Al_2O_3$), depending on the threat and weight constraints (Navarro *et al.* 1993). The ceramic layer acts to blunt and wear down the projectile. The ceramic layers need to be supported by a more flexible backing layer that also function to catch the slowed remnants of the projectile while keeping the integrity of the system (Hogg 2003). Polymer composites fulfill those requirements and bond well with the ceramic and other layers to form an integral armor system with lightweight. In addition to composite backing plates most integral armors contain an additional external fiber composite layer covering the ceramic tiles to protect them from minor damages. For the design of integral armor, glass fibers (S-2 glass, E-glass) are being employed with epoxy, vinyl ester and polyester resin systems due to their high tensile and compressive strength, good energy absorption properties and relatively lower costs (High Performance Composites 2005). Also, an additional elastomer layer has been reported to be added behind the ceramic tiles for shock attenuation to improve the multi-hit capacity of the armor (Gama *et al.* 1999, Gama 2001, Tanoğlu *et al.* 2001, Vaidya 2001). Figure 2.5 is a schematic representation of a typical multilayered integral armor system. The components of the armor are: (a) Durability cover for outer shell comprising S2-glass reinforcement, (b) Ceramic tiles for ballistic protection, (c) Ethylene propylene diene monomer (EPDM) rubber for multi-hit damage tolerance, (d) Thick section composite structural laminate which is the primary structural load bearing component, (e) Electromagnetic interference (EMI) mesh for electromagnetic shielding, (f) A Phenolic laminate liner for flammability protection.

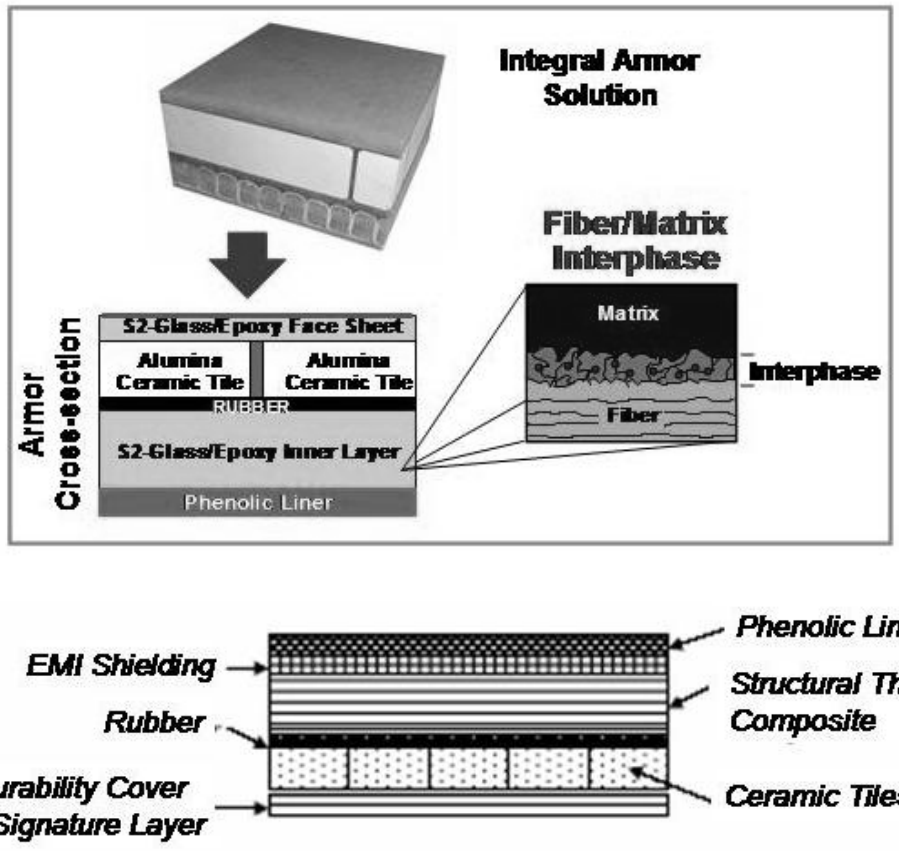


Figure 2.5. Representative of integral armor design (Source: Tanoğlu *et al.* 2001, Vaidya 2001).

The penetration resistance of fiberglass reinforced plastic plates under ballistic impact was investigated by Wang (Wang *et al.* 1997). In that study two forms of E-type glass fibers were used: woven roving and chopped strand mats and also two types of resin were used in making the composite: vinyl ester and epoxy. In this investigation, it was reported that the fabricated composites were not suitable for defeating high-speed armor-piercing rounds when used alone. Instead, they should be used with some hard materials, such as ceramic tiles, which would reduce the impact velocity significantly. However, they might be effective against fragments.

In composite integral armor design, there are some critical factors that affect the ballistic resistance of the composite structure. Obliquity of impact, areal density of the materials and impact velocity are important to investigate the mechanism of penetration. If the mechanism of the penetration is understood, design of the composite armor against the ballistic threat would be more easy and simple. Besides, optimization of the front plate to back plate thickness ratio, is a key point to design of the integral armor (Elperin *et al.* 2000a, Elperin *et al.* 2000b, Wang and Lu 1996). For this purpose

numerous investigations were conducted. On the other hand it is known that experimental research is expensive and takes time to change the conditions for the investigations. A number of simulation techniques are employed to optimize the parameters to develop advanced armor. Benloulo *et al.* studied the impact onto the ceramic/composite armor (Benloulo *et al.* 1998). A simple analytical model of impact onto the ceramic/composite was developed. The model is divided into three phases of penetration: intact ceramic, fractured ceramic and initial response of the composite substrate, and fabric response and failure. It was reported that predictions from the combined model are in relatively good agreement with a limited set of experimental data. Hetherington investigated the optimum thickness of two component composite armors (ceramic/aluminum) using Florence model (Hetherington 1992). It was reported that a development of the Florence model permits a prediction of the ratio of front to back plate thickness for optimum performance of two component armor systems. Sadanandan *et al.* investigated the ceramic/steel and ceramic/aluminum armors (Sadanandan *et al.* 1997). In this study, it was represented that the ballistic limit velocity ($V_{50}$) increased with obliquity and they characterized the oblique impact of ceramic/metal armor. Also, Zaera *et al.* studied normal and oblique impact on ceramic/metal armor (Zaera *et al.* 1998). They developed an analytical model to simulate ballistic impact of projectiles on ceramic/metal add-on armors. The model permits a fast computation of ballistic limits, residual velocities and residual masses, being a useful designing tool for ceramic/metal armors. The model was utilized both for small caliber projectiles and medium caliber projectiles, perforating different ceramic/metal targets at different impact angels. Navarro *et al.* investigated the influence of the adhesive in the ballistic performance of ceramic faced plate armors (Navarro *et al.* 2000). It was presented that the thicker layer of adhesive gives rise to a larger area of plastic deformation of the metallic plate, which helps to absorb the kinetic energy of the projectile. Also, the study revealed that the ceramic tile is shattered earlier when the adhesive layer is thicker.

## 2.3. Ballistic Limits of Composites and Projectile Armor Interactions

Fiber reinforced polymer composites have been used in numerous military applications that they can replace metals, ceramic and other ballistic materials. The

ability of a material to provide a useful contribution to an impact event depends on the hardness of the materials which is critical for blunting a projectile. Also, the strain to failure which determines the ability of that material to absorb energy via a global deformation process affects the impact event. Deformation process involves either brittle cracking in the case of ceramics and composites, or plastic deformation in the case of some metals (Hogg 2003).

According to Hogg (Hogg 2003) composite materials rely primarily on brittle micro fracture events to absorb energy. This means that the ultimate energy absorption is largely controlled by the strain to failure of the fibers. Once the fibers have ruptured the armor collapses and no further energy is absorbed. Fibers might be expected to absorb energy via plastic deformation and drawing of the fibers. This process can happen effectively in dry un-impregnated fibers arranged in a textile form, but the ability of the fiber to deform in this way is severely restricted in a composite and energy absorption can be disappointing. In Figure 2.6 it can be seen that the load conditions on woven fabrics. And also the behavior of the fiber under impacting of the projectile was represented in Figure 2.6.

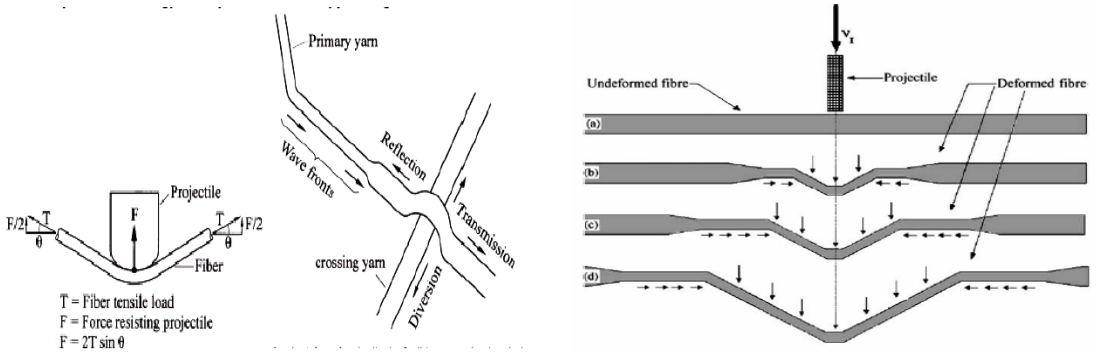


Figure 2.6. a) The load conditions on fibers in a woven textile during penetration rupture, b) Configuration of a yarn/fiber before and after transverse impact (Source: Hogg 2003, Naik 2004).

When an armor-grade composite is impacted, if the projectile possesses sharp edges and/or the composite properties are somewhat brittle and/or there is an increased level of fiber/matrix adhesion, the first few plies may be sheared out, forming a plug. After the plug is formed, sequential delamination was noted, along with fiber pull-out and fiber tensile failure in the back layers of the laminate. Lateral movement of fibers was observed for unidirectional cross-ply laminates, but not seen in fabric laminates.

Fibers are driven into the underlying layers before they fail, rebound and form a reverse pyramid on the impact surface. Beneath the projectile, the material is compressed and the remaining layers form a membrane, which absorbs the remaining energy through fiber elongation and fiber pull out (Figure 2.7) (Cheeseman *et al.* 2003).

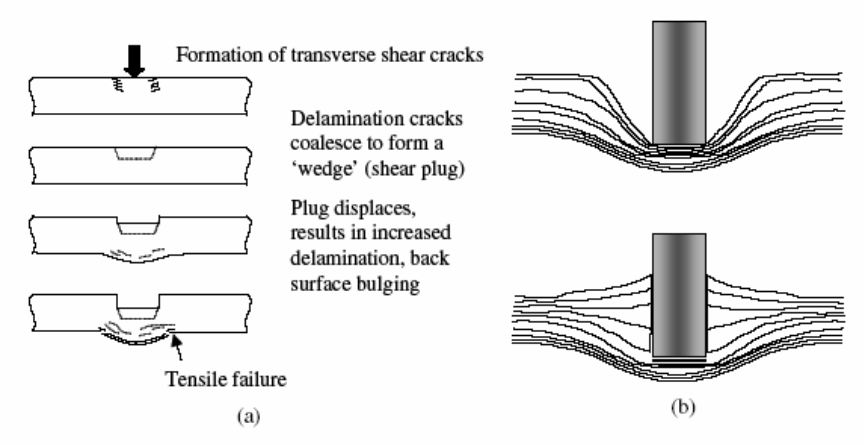


Figure 2.7. Penetration into compliant laminates (a) with shear plug formation and (b) with compaction and spring-back (Source: Cheeseman *et.al.* 2003).

Gellert and coworkers investigated the effect of target thickness on the ballistic perforation of glass-fiber reinforced plastic composites (Gellert *et al.* 2000). They measured ballistic resistance of the laminate under impacting different nose shape projectiles and sectioned the perforated laminates. They represented two characteristic patterns of damage or delamination for thin and thick laminates illustrated in Figure 2.8. For thin targets the damage was in the form of a cone of delamination opening towards the target exit side. This cone increased in diameter and height with increasing target thickness, until with sufficiently thick targets a cone of delamination opening towards the impact side.

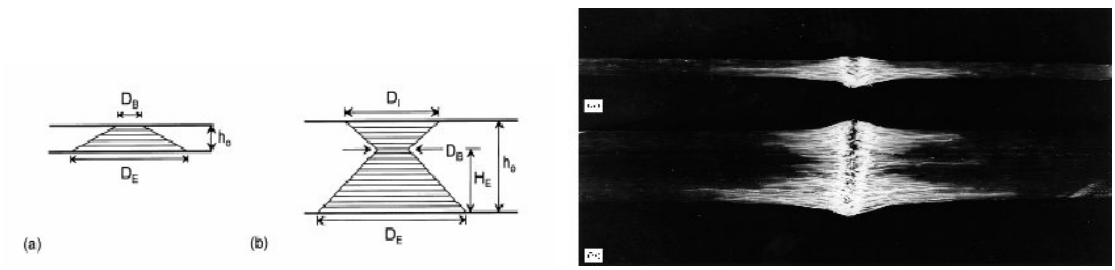


Figure 2.8. The schematic geometry and photograph of damage zone of the thin and thick composite (Source: Gellert *et al.* 2000).

The ballistic impact performance of polymer-based composite materials bonded to Al-substrate was experimentally investigated as an alternative to the conventional steel product by Fındık (Fındık *et al.* 2002). The results obtained from the investigation was; the thinner composite plates have higher elasticity than the thicker ones in the ballistic testing, the bending and tensile strength are increased with the increments of composite layers and the velocity of the bullet is decreased with the increment of layer numbers. In contrast, output is obtained as the opposite behavior of speed. Another result is that the depths of trace of the bullets are decreased with the increment of the layer numbers. Also, there is a direct proportionality between speed and the trace depth for all layer numbers. In addition, the penetration depth is increased with the increment of bullet speed.

The ballistic properties of gel-spun polyethylene (GSPE) fiber composites were investigated by Warda (Warda *et al.* 1999). In this study, two different manufacturing process were used; conventional prepreg route and hot compaction route. Examination of these composites after ballistic testing showed that the energy was absorbed via fiber failure and back-face delamination. The back-face delamination decreased at higher compaction temperatures because of increased interfacial bonding resulting in a decrease in the ballistic performance.

Bhatnagar and coworkers studied ballistic performance of the composite structures made with combinations of the fibers and resin systems (Bhatnagar *et al.* 1989). In their study, ballistic performance of glass, aramid, Spectra and Spectra/glass hybrid composite laminates were compared. Also the hybrid laminates of Spectra/glass/VE and glass/spectra/VE was tested and the laminate performed better if glass face was shot instead of the Spectra face. This was due to the fact that Spectra fiber has a higher energy absorption rate in tension. The results showed that Spectra/VE shell provided better protection against fragment than Spectra/glass/VE, glass/spectra/VE or aramid/phenolic/PVB.

## 2.4. Prediction of Ballistic Behavior of Composite Laminates

A number of studies were performed for the prediction of the penetration and perforation FRP laminates. Wen investigated the penetration and perforation mechanisms of thick FRP laminates (Wen 2000 and Wen 2001). In their study,

analytical expressions are derived for the penetration and perforation of FRP laminates by rigid projectiles with different nose shapes. The approach is based on the assumption that the deformations are localized and that the average pressure provided by the target materials to resist the projectiles can be divided into two parts. One part is the cohesive quasi-static resistive pressure applied normally to the projectile surface due to the elastic-plastic deformations of the FRP laminate materials. The second one is the dynamic resistive pressure arising from velocity effects. This latter is simply expressed as a velocity-dependent enhancement factor applied to the static pressure term. Correlation between the equations and the available experimental data is presented and discussed.

### 2.4.1 Penetration of Semi-infinite FRP Laminates

Figure 2.9 shows the geometries of rigid projectiles with conical and ogival noses based on the study of Wen (Wen 2000 and Wen 2001). The projectiles are assumed to have density $\rho_p$ and mass $G$ with diameter $D$ (or radius $a$), $L$ and $L_N$ are the lengths of the shank and nose for ogival and conical projectiles as shown in Figures 2.9 (a) and (b), respectively. Figure 2.9 (a) shows the ogive profile as the arc of a circle that is tangent to the projectile shank. It is also common to define the ogive in terms of caliber-radius-head:

$$CRH = \frac{S}{2a} = \psi \,, \tag{2.1}$$

where $S$ and $a$ are defined in Figure 2.9 (a). If a rigid projectile has a complex configuration (for example, it is hollow or has a sabot system) then the projectile still can be described as one of those depicted in Figure 2.9 but with an effective density ($\rho_p^e$) which is taken to be the ratio of the projectile mass to the volume of the basic configuration as shown in Figure 2.9.

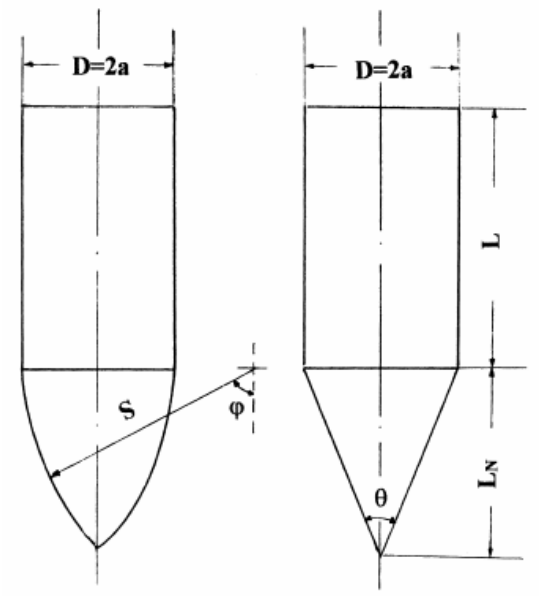


Figure 2.9. Projectile geometries: (a) ogival nose and (b) conical nose (Source: Wen 2000).

Figure 2.10 shows the impact of a rigid projectile with a conical nose on an FRP laminate target at normal incidence with an initial impact velocity *Vi*. Two situations may arise depending upon the initial kinetic energy of the projectile, as shown in Figure 2.10. Equations are shown in the following sections for the depth of penetration into the FRP laminate targets by rigid projectiles with conical and ogival noses.

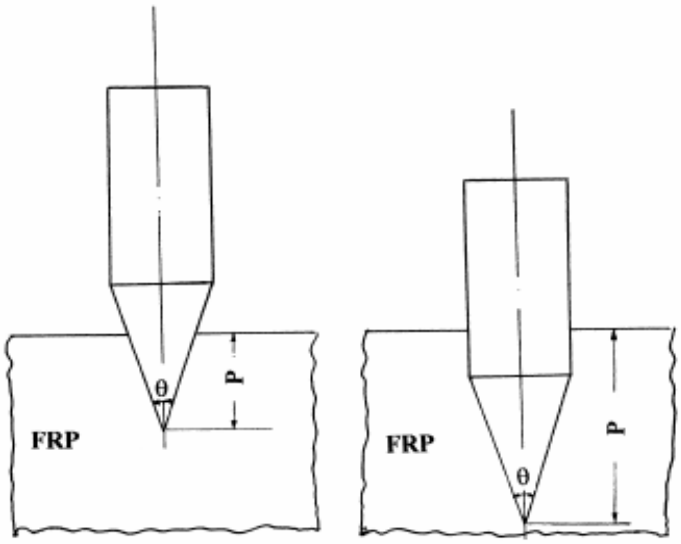


Figure 2.10. Schematic diagrams of a conical-nosed projectile impacting on semi-infinite FRP laminate targets. (a) P ≤ $L_N$; (b) P > $L_N$ (Source: Wen 2000).

**Conical-nosed projectiles**

For a rigid conical-nosed projectile, the motion and the final depth of penetration can be calculated if the resistive forces are known.

From energy conservation and rearranging the formula given by equation (2.1), (2.2), (2.3).

for case I, P≤$L_N$

$$\frac{P}{L+\frac{L_N}{3}}=\left(\frac{\rho_p}{\rho_t}\right)\frac{\rho_t V_i^2}{\sigma_e}\frac{1}{\frac{2}{3}\left[1+\beta\sqrt{\frac{\rho_t}{\sigma_e}}V_i\right]\left(\frac{P}{L_N}\right)^2} \tag{2.2}$$

for case II, P>$L_N$

$$\frac{P}{L+\frac{L_N}{3}}=\left(\frac{\rho_p}{\rho_t}\right)\frac{\rho_t V_i^2}{\sigma_e}\frac{1}{2\left[1+\beta\sqrt{\frac{\rho_t}{\sigma_e}}V_i\right]}+\frac{2}{3\left(\frac{L}{L_N}\right)+1} \tag{2.3}$$

can be derived.

## 2.4.2 Perforation of Finite FRP Laminates

Based on the study of Wen (Wen 2000 and Wen 2001) the ballistic limit condition for an FRP laminate with finite thickness struck transversely by a rigid projectile with conical or ogival noses can be estimated by the energy balance method. There are three phases of penetration for a rigid projectile with conical nose impacting on a finite plate. First, the nose enters the plate, second, the nose is fully embedded and finally, the nose exits the plate.

$V_b$ is the critical impact velocity or ballistic limit can be represented as equation (2.4).

$$V_b=\frac{\pi\beta\sqrt{\rho_t\sigma_e}D^2T}{4G}\left[1+\sqrt{1+\frac{8G}{\pi\beta^2\rho_t D^2T}}\right] \tag{2.4}$$

# CHAPTER 3

## RESIN TRANSFER MOLDING (RTM) TECHNIQUE

### 3.1. Principle of the RTM Process

Resin transfer molding (RTM) is a closed-mold low pressure process that allows the fabrication of composites ranging from simple, low-performance to complex, high-performance articles and in size from small to very large (Johnson 1987).

Figure 3.1 shows the schematic of the RTM process. In the RTM method, fiber reinforcement, is placed into a mold cavity. Individual fabrics or fiber preforms may be used in RTM mold (Lee *et al.* 2002, Hillermeier 2001)**.** The fiber volume fraction ($v_f$) of reinforcement in the range of 0.3-0.6 is used for RTM for the easy flow of a resin and impregnation of a reinforcement (Advani 1994). Once the mold is closed, resin mix is transferred into the mold cavity through injection ports at a relatively low pressure. Injection pressure is normally less than 690 kPa (or 100 psi). The displaced air is allowed to escape through vents to avoid dry spots. Cure cycle is dependent on part thickness, type of resin system and the temperature of the mold. The part cures in the mold, normally heated by controller, and is ready for its removal from the mold when sufficient green strength is attained (Fong *et al.* 1998). The cycle time of large parts of uniform thickness is often 3 min or less using heated tools (Johnson 1987). RTM technique offers production of low cost composite parts with complex structures and large near net shapes.

The structural reaction injection molding process (SRIM) is similar to the RTM process. It also uses a preform that is placed in the tool before the introduction of the resin system. The resin is highly reactive and the overall pressure of the resin is about 340-690 kPa. The resin flows into the tool and wets out the preform as the curing is occurring. The cycle time is around 1 min resulting in the rapid curing. Because of the rapid resin cure, flow distances are limited in this process. When flow distances exceed 610 mm, multiple inlet ports are desirable. Reinforcement levels used in this process is typically to be 5 to 55 wt%. (Johnson 1987).

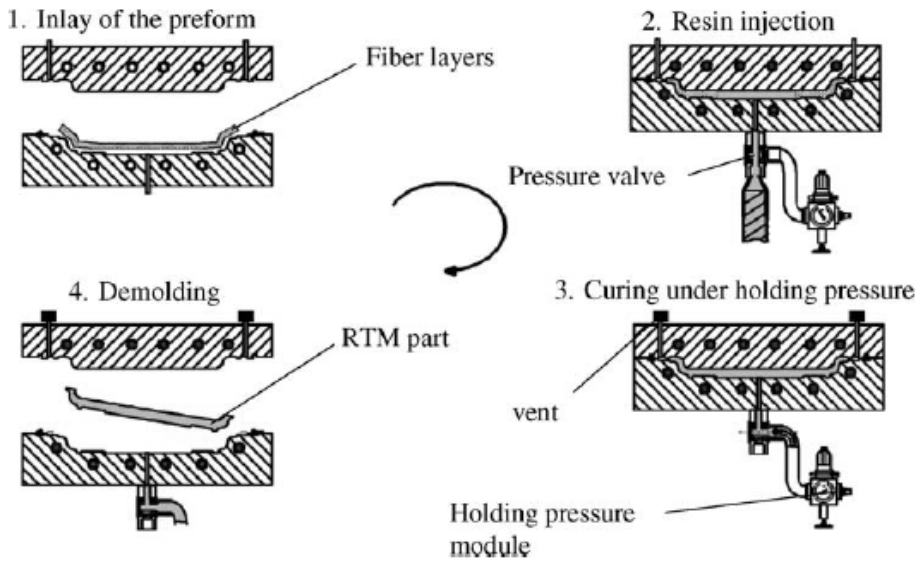


Figure 3.1. Resin transfer molding process (Source: Schmachtenberg *et al.* 2005)

The advantages of RTM can be summarized as below (Strong 1989, Jang 1994, Hull 1995):

1. For rigid tool RTM all dimensions including part thickness are controlled by the tool cavity.
2. Surface definition is superior as compared to lay-up technique. Surface finish replicates that of the tool; generally a smooth finish is chosen for advanced work.
3. A combination of reinforcements, such as 3D wovens, stitched assemblies and braids, can be used to meet specific properties.
4. A wide variety of resin systems can be utilized.
5. Very large and complex shapes can be made efficiently and inexpensively through the use of preforms.
6. Production cycles are much shorter than lay-up technique.
7. For fixed cavity tooling, fiber volume fractions can be very well controlled, leading to very consistent mechanical properties.
8. Inserts and special reinforcements can be added easily.
9. Volatile emissions are low because RTM is a closed mold process.

Disadvantages of RTM:

1. The mold design is critical and requires great skill. Improper gating or venting may result in defects.
2. Properties are equivalent to those with matched die molding and not as good as with vacuum bagging, filament winding or pultrusion.
3. Control of resin uniformity is difficult. Radii and edges tend to be resin rich.
4. Reinforcement movement during resin injection is sometimes a problem.

### 3.1.1. Materials for RTM

Fiber types used with RTM include E, R & S glass, quartz, a wide variety of high-strength and high-modulus carbon fibers and aramids. Conventionally, woven cloth is the most common used reinforcement type, and is available in staggering variety of materials, weaves and weights. A variety of non-crimped cloth constructions are available that aim to reduce or remove the crimping of fiber tows inherent in woven cloths and thus improve mechanical properties (Potter 1997). Multi axial fibers enable production of parts with higher fiber volume because uncrimped fibers facilitate better resin flow and the basic structure nests fiber bundles closer to one another, eliminating the interstices where resin accumulates in wovens and chopped strand mats (WEB_2). The types of fibers that are used in RTM are represented in Figure 3.2.

On the other hand, natural fibers such as hemp, jute, flax, kenaf or sisal can be used in RTM. The composites containing natural fibers has advantages compared to synthetic fibers reinforced plastics such as low tool wear, low density, cheap cost, availability and biodegradability. Despite the fact that having many advantages, the natural fibers are not suitable using above 160 $^{o}$C because of thermal degradation. Also, the moisture content, which caused the voids in the matrix, of the natural fiber effects the final properties of the composites (Rouisona et.al 2004, Sebe et.al 2000).

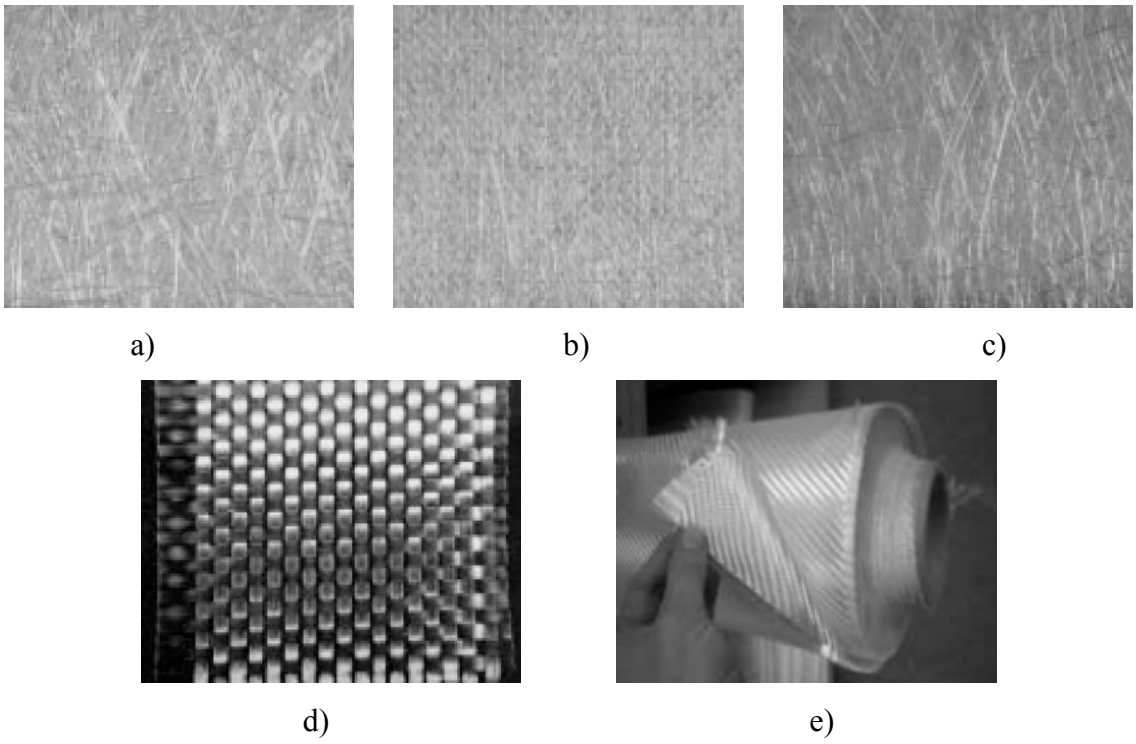


Figure 3.2. Photographs of reinforcing fabrics: a) Powder-bonded chopped-strand mat b) Stitch-bonded chopped-strand mat c) Continuous-filament mat d) Plain weave fabric from glass fiber rovings e) Multiaxial non-crimb fabric.

There are several resin systems that perform adequately in an RTM process. Table 3.1 summarizes the relative advantages and disadvantages of polyester, vinyl ester, and epoxy resins. Polyester is the most commonly used resin because of its low cost. Polyester resin properties vary strongly with chemical formulation but generally they offer a high performance per cost ratio. Epoxy has been used in many applications such as aerospace and consumer products and has been demonstrated to provide high physical properties, mid-range price. Vinylester resin provides properties between those of polyester and epoxy at a moderate price for RTM technique and also they have better adhesion and fatigue properties than polyester (Johnson 1987, Warrior *et al.* 2003). Phenolic resins are normally used where a combination of low cost and fire resistance is demanded. Bismaleimides offer the heat and fire resistance of phenolics, coupled with the ease of processing, convenience and the level of properties of epoxies: at a price higher than either (Potter 1997).

For all of the resin systems, a low-viscosity plateau is required during which the resin can provide constant flow throughout the mold followed by a fast cure. In practice a viscosity below 10 poise is preferred and many RTM resins have much lower

viscosities. The resin is required not only gel rapidly for an acceptable rapid RTM cycle, but also provide sufficient Barcol Hardness to allow the component to be demolded without distortion.(Johnson 1987**,** Potter 1997, Brouwer *et al.* 2003, Ferret *et al.* 1998).

Table 3.1. Thermosetting resin comparison (Source: Monib 1998).

| Resin System | Advantages | Disadvantages |
|---|---|---|
| Polyester | • Low cost<br>• Easy to process<br>• Good chemical and moisture resistance<br>• Fast cure time<br>• Room temperature cure | • Flammable<br>• Toxic smoke upon combustion<br>• Average mechanical properties |
| Vinyl ester | • Low cost<br>• Ease of processing<br>• Low viscosity<br>• Room temperature<br>• Moisture resistant<br>• Good mechanical properties | • Flammable<br>• Smoke released upon combustion<br>• Mechanical properties is not good as epoxies |
| Epoxy | • Excellent mechanical properties<br>• Good chemical and heat resistance<br>• Good adhesive properties with a large variety of substrates<br>• Moisture resistant<br>• Variety of compositions available<br>• Good fracture toughness | • Expensive<br>• Requires high processing temperatures to achieve good properties |

## 3.2. Critical Parameters on RTM and Part Quality

Design of the mold (including gate dimensions, heat-up rates of the tool, tool stiffness) and cycle time are very critical issues for production and quality in RTM. In most variants of RTM the tooling is solely responsible for the geometry and tolerances of the part. The tool dictates how the resin will enter and leave the part and in very large part controls the filling process and thus the quality of the components. On the other hand, the behaviour of the resin flow, resin input pressure, shrinkage of resin after curing, warpage problem, tow, fiber wet-out rates, fiber volume fraction ($V_f$) and mold fill time are the critical factors that affect the quality of the part and characterize the RTM process (Potter 1997, Kim *et al.* 2002).

All of the factors mentioned above are correlated with each other. As the fiber volume fraction increases, the sizes of the micro channels within fibrous texture through which resin can flow become smaller. The permeability of preform is decreased. Thus, high fiber volume fraction leads to a slow resin flow during resin impregnation into the preform, subsequently increasing the process time. Higher injection pressure enables faster resin flow, but the preform may be deformed or washed out for excessively high injection pressures. Therefore, mould filling in RTM becomes difficult with increasing the fiber volume fraction (Kang *et al.* 2000).

Altan and co-workers (Altan *et al.* 2004) investigated the effect of preform thickness and volume fraction on injection pressure and mechanical properties of RTM composites. They observed that mechanical properties of the composites increase with the increase of fiber volume fraction. Increase of fiber volume fraction from 6.84 to 24.83% leads to 150% increase of ultimate tensile strength, and 100% increase of elastic modulus and short beam shear strength of the composites. Also, they observed that permeability values measured for thin mats were higher than values of thick mats at about 48-227%; meanwhile it was obtained that injection pressure reduced in the range of 40-70%.

The relationship between the factors that affect the mold fill time can be seen from equations 3.1 to 3.5 developed to relate the infiltrated resin volume with respect to time. Fiber volume fraction ($V_f$), inlet area in RTM ($A_0$), inlet pressure in RTM ($P_0$), mold thickness based on $V_f$ ($h$), longitudinal permeability at $V_f$ ($S_x$), transverse permeability at $V_f$ ($S_z$), flow front position in the longitudinal direction ($Z_f$) and viscosity

of the resin ($\mu$) are the factors that effect the mold filling in RTM. Choi *et al.* explained the flow of the resin in two regions in the mold; before and after the resin front reaches the bottom of the mold. The time when the resin front reaches the bottom is denoted by $t_c$ and total infiltration resin volume at a given time can be explained as in (Equation 3.1-3.2) (Choi *et al.* 2002).

$$Q = (1 - V_f)\left[\frac{1}{3}\sqrt{C_1 C_2}\cdot t + A_0\sqrt{C_2 t}\right] \quad \text{for} \qquad t \le t_c\left(=\frac{h^2}{2C_2}\right) \tag{3.1}$$

$$Q = (1 - V_f)\left[\frac{1}{3}\sqrt{C_1 C_2}\left(1-\left(1-\frac{h}{z_f}\right)^{3/2}\right)t + A_0\sqrt{C_2 t_c}\right] \quad \text{for} \qquad t \ge t_c \tag{3.2}$$

where,

$$C_1 = \frac{2S_x P_0}{\mu(1 - V_f)} \tag{3.3}$$

$$C_2 = \frac{2S_z P_0}{\mu(1 - V_f)} \tag{3.4}$$

$$Z_f = \sqrt{\frac{2S_z P_0 t}{\mu(1 - V_f)}} \tag{3.5}$$

The resin temperature may be elevated by heating the mould. If the resin is heated the viscosity decreases and thus the flow speed is increased. Due to the heat transfer from the mould to the thermosetting resin, cure reaction takes place during the mould filling and the time required for the post-curing can be reduced. Then, the heated mould reduces the total manufacturing time by accelerated curing as well as the reduced resin viscosity. However, if the resin temperature is raised excessively, the gelation of resin may be reached too fast and the resin flow may prematurely stop before the completion of mould filling. A more effective method for enhancing the flow is to use multiple injection gates (Kang *et al.* 2000).

Another problem in RTM is the race-tracking phenomenon. The race-tracking can dramatically change the resin infiltration process. It can be explained as flowing of the resin faster along the minuscule channels induced by imperfect fits between the preform edges and the mold walls. The ramifications of race-tracking are that the resin may arrive at the vents before completely impregnating the preform and create undesired dry spots, which are fiber regions devoid of resin. The strength and existence of race-tracking is a function of operator skill, variability in preform architecture, the fabric type, perform manufacturing method, and their placement in the mold. It can vary from one part to the next in the same production run and generally it is not repetable (Hsiao *et al.* 2004, Devillard *et al.* 2003).

Experiences show that foulness of fiber placement into the mould cause to form small clearance of 1 or 2 mm between the preform and mold wall; and these channels could have significant effect to resin flow, especially if the preform has high fiber content. Trochu and co-workers (Trochu et.al, Hammami et.al 1998) investigated edge effect on flow patterns in RTM. They presented a model that describes this channeling effect in computer simulation of the mold filling process. This model characterizes the flow in the channel and through the reinforcement. The channel width and permeability of the reinforcement are significantly effective on the resin flow.

Durant *et al.* (Durant *et al.* 2003) reported in their study that two-part Room Temperature Vulcanizing Rubber (RTV) was used to seal the inside edges of the mold near the ends of the fibers. These inserted baffles were used to force the resin to flow through the fibers instead of around the edges of the mold. This eliminated the dry spot and race-tracking problem and flawed parts were no longer produced.

Thermal deformations are also critical on the RTM part quality; the fibers possess a small thermal expansion coefficient along their longitudinal axis and that produces little deformation during resin cure. On the other hand, having a much higher thermal expansion coefficient of polymer matrix causes the composite structure to be effected by the temperature changes and thus different thermal behaviors produce the residual stresses. Meanwhile, the residual stresses which are generated during curing of resin affect the mechanical properties and quality of parts. Residual stresses are also the reason of producing of warpage, matrix cracks or delamination. If the composite structures are thick enough to be rigid, matrix damage occurs instead of distortion of the composites. The lower the temperature, the lower the residual stresses in RTM process. From another point of view to initiate the cross-linking chemical reaction, the

temperature must be reached at a minimum level. If the temperature is lower than optimum level the cure reaction takes longer; and in this case mechanical properties may be affected (Ruiz *et al.* 2005).

At present, much of the tooling, preform design, and process development for a new RTM part is done by trial and error. Expensive modifications on the tool are unavoidable if the tool and preform have inaccuracies during the design period. Extensive research were presented in the literature about the developing mathematical models that can describe the flow behaviour of resins through the different molding tools loaded with different architectures. These kind of research aim to characterize the physical and chemical changes that occur during the RTM process (Advani *et al.*1994).

Simulation of the molding process can predict flow fronts, allowing engineers to virtually test different mold designs without building expensive hardware. Modeling of the flow front depends on a large number of variables, including preform geometry and permeability; resin temperature, viscosity, pressure, and cure state (all of which vary with both time and position); mold geometry; heating elements; and the location of injection ports and vent.

A few commercial programs are available for the simulation of molding process. The PAM-RTM program from ESI Group simulates the entire molding process before the tooling is made. The simulation allows the user to find optimum configurations that minimize molding time, resin waste and other costs. A similar program, RTM-Worx from Polyworx provides simulation of both RTM and vacuum infusion process (High Performance Composites, Manufacturing Control Software, November 2003, pp.18-22).

Lee *et al.* (Lee *et al.* 2002) investigated the injection strategies using multiple injection gates to facilitate the resin flow during mould filling process of RTM. A numerical code was developed to simulate the resin transfer mould filling process with multiple injection gates. Experiments were also performed for different injection schemes, the results of which show close agreement with the numerical predictions. The multiple gate injection methods were found to be effective for reducing the mould filling time (Kang *et al.* 2000).

# CHAPTER 4

## EXPERIMENTAL

### 4.1. Materials

E-glass $0^o/90^o$ woven fabrics and isophthalic polyester thermosetting resin (Camelyaf 266) were purchased from Cam Elyaf Corporation of Turkey to fabricate composite armor panels. In addition, E-glass $0^o/90^o$ biaxial and $0^o/+45^o/-45^o/90^o$ quadraxial stitched non-crimp fabrics (Telateks A.Ş., Turkey) and orthophthalic polyester thermosetting resin (Herkim A.Ş., Turkey) were used to fabricate composite plates. The woven fabrics and non-crimp fabrics can be represented in Figure 4.1.As an accelerator 0.28 wt. % of cobalt naphthenate (CoNAP) and as initiator 1.5 wt. % methyl ethyl ketone peroxide (MEKP) were added to the polyester resins. Ceramic alumina 95 ($Al_2O_3$) tiles (DMS, Germany, 9 Mohs schale typical hardness) or metallic Al plates, in the dimensions of 100x100 mm, were added to polymer composite panels to improve their ballistic performance. The mechanical properties of ceramic alumina 95 ($Al_2O_3$) tiles are summarized in the Table 4.1. Silane coupling agent (3-Methacryloxypropyl trimethoxysilane, purchased from Aldrich) was applied to alumina surfaces to improve the adhesion.

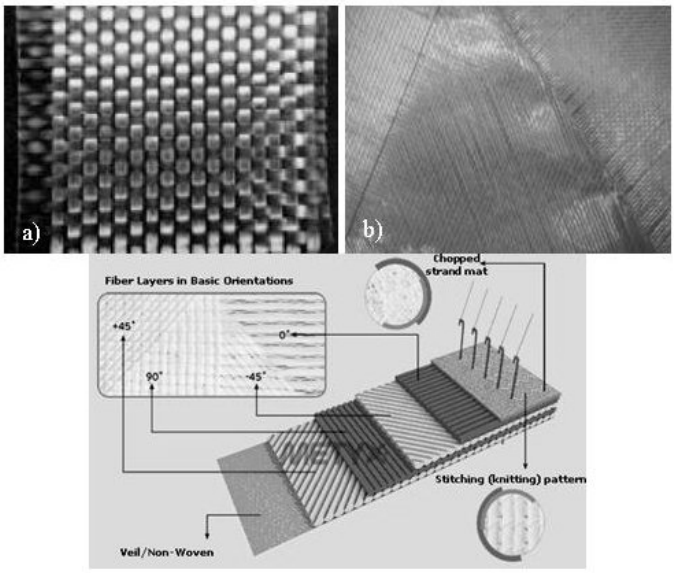


Figure 4.1. The schematic representation of woven and non-crimp fabrics: a)Woven fabrics b) Multiaxial non-crimp fabrics (Source: WEB_3)

## 4.2. Surface Modification of Ceramic Tiles

Alumina tiles were treated with silane coupling agent to improve the adhesion between the polymer and ceramic surfaces. An aqueous solution of the silane was prepared by adding 0.5 wt. % of silane (3-Methacryloxypropyl trimethoxysilane, purchased from Aldrich) into deionized water that its pH was adjusted to about 4 by adding acetic acid. The solution was stirred with the help of a magnetic stirrer for about 1 hour to obtain the hydrolysis of the silane. The alumina tiles were deep coated with silanol solution for about 15 minutes. To form siloxane on the surfaces, alumina tiles were dried at 90$^{o}$C for 30 minutes in an oven. In order to observe the uniformity of the coatings, the surfaces of the alumina tiles were examined with a field emission gun scanning electron microscope (SEM). Figure 4.2 represents the schematic of surface modification of ceramic tiles.

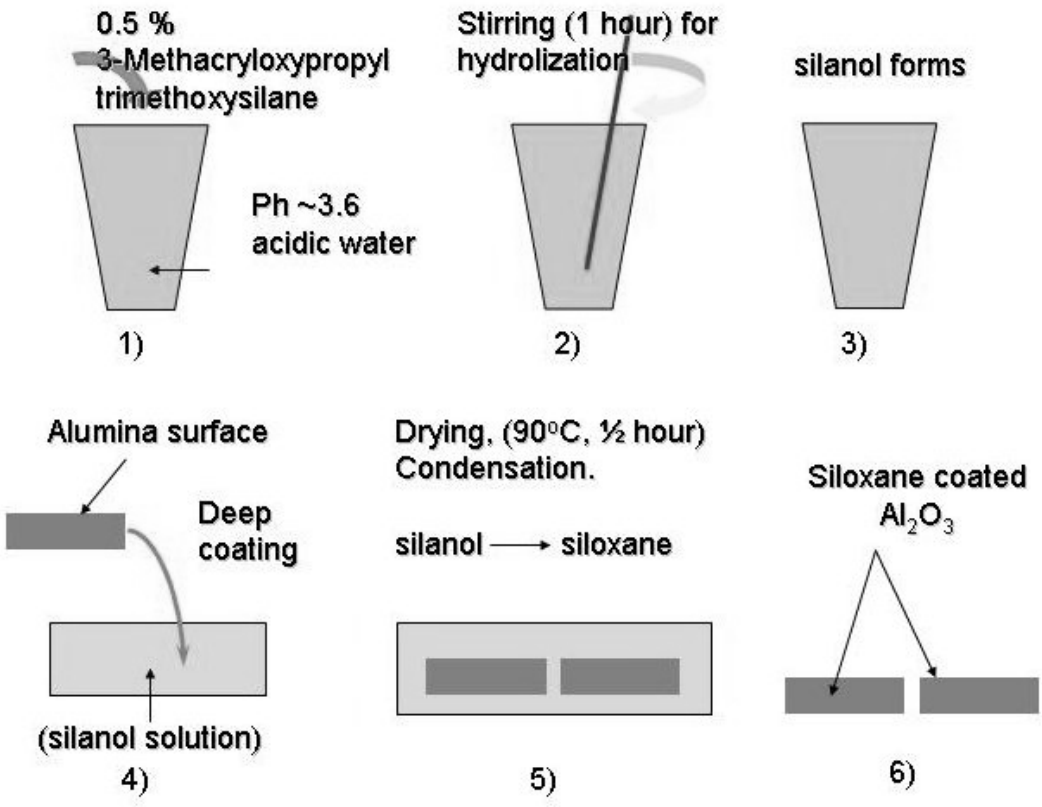


Figure 4.2. Schematic of surface modification of ceramic tiles.

## 4.3. Fabrication of Composite Armor Panels

The composite panels were manufactured using RTM technique (Figure 4.3.). In this technique, dry glass fabrics cut in 300x300 mm dimensions were placed into a RTM mold cavity which were applied the mold release agent (wax-SV8) on the surfaces. After the placement of the fabrics, the mold was closed and clamped tightly, and then the resin was injected into the mold cavity. After completion of the resin injection and curing, the parts were demolded and transferred into an oven for post curing at 110$^{o}$C for 2 hours. Ballistic test panels with various areal densities (mass per unit area) were fabricated with and without Al and $Al_2O_3$ tiles. In addition to the woven fabric/polyester composite laminates, the non-crimp/polyester composite laminates were produced. Furthermore, composites were fabricated for testing the mechanical properties.

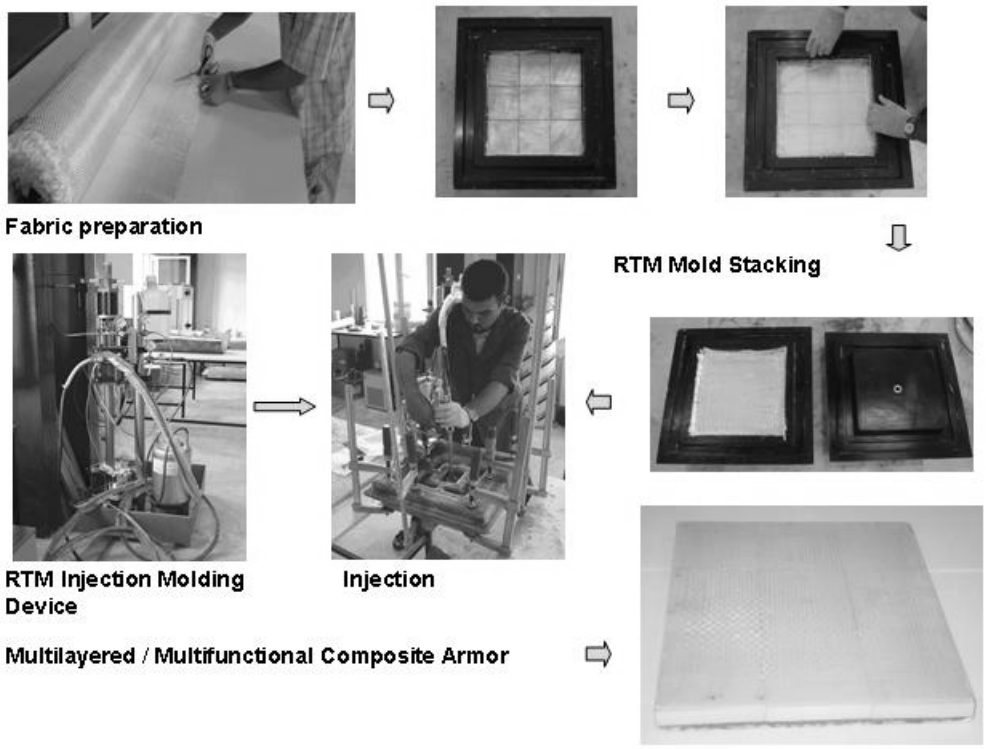


Figure 4.3. The stages of fabrication of lightweight composite armor panels.

## 4.4. Measurement of Fiber Volume Fraction

The burn-out test method was used to determine the fiber volume fraction of the E glass/polyester panels. In this method, sample of about 0.1-0.5 g. of composite is burned off in a high temperature oven. The remaining fiber is weighed and the volume of the fiber is calculated using equation 4.1. The density of each component is taken from the literature and void content was assumed to be negligible. The weight fractions allow derivation of an approximate fiber volume fraction ($V_f$) as below

$$\vee_f = \frac{V_f}{V_f + V_m} \times 100 = \frac{(\frac{m_f}{\rho_f})}{(\frac{m_f}{\rho_f} + \frac{m_m}{\rho_m})} \times 100 \qquad (4.1)$$

where $V_f$ and $V_m$ are volume of fiber and matrix, $m_f$ and $m_m$ are mass of fiber and matrix and $\rho_f$ and $\rho_m$ are density of fiber and matrix, respectively.

## 4.5. Microstructure Characterization

Scanning electron and optical microscopy on the fracture surfaces of tested specimens were performed in order to investigate the failure modes. For this purpose, Phillips™ SEM and Nikon™ optical microscopes were used. Moreover, ballistic damage modes in the panels were observed for composites and alumina tiles. For that reason, ballistic test panels were cross-sectioned through the impacted zones using diamond saw. The cross sections of the panels were prepared by metallographic techniques.

## 4.6. Mechanical Property Characterization

### 4.6.1. Flexural Properties

The flexural test technique, ASTM D 790M-86 was used to determine the flexural strength and modulus of the composites. For this purpose, test specimens with 10 mm in width, 6mm in depth and 125 mm in length were sectioned from the RTM panels using a diamond saw. Specimens were tested in 3-point bending apparatus with a span to thickness ratio of 16. Figure 4.4 shows the flexural test specimen. At least five

specimens from composites were tested using the universal test machine at a crosshead speed of 2.6 mm/min. Force vs. deflection at the center of the beam was recorded. The flexural strength, *S*, values were calculated from;

$$S = 3PL/2bd^2 \tag{4.2}$$

where *P* is the applied load at the deflection point, *L* is the span length; *d* and *b* are thickness and width of the specimen, respectively. The maximum strain in the outer fibers occurs at midspan and calculated as,

$$r = 6Dd / L^2 \tag{4.3}$$

where *r* is the maximum strain in the outer fibers, *D* is the deflection. The flexural modulus values, $E_b$ were calculated from;

$$E_b = \frac{L^3 m}{4bd^3} \tag{4.4}$$

where *m* is the slope of the tangent to the initial straight line portion of the load-deflection curve.

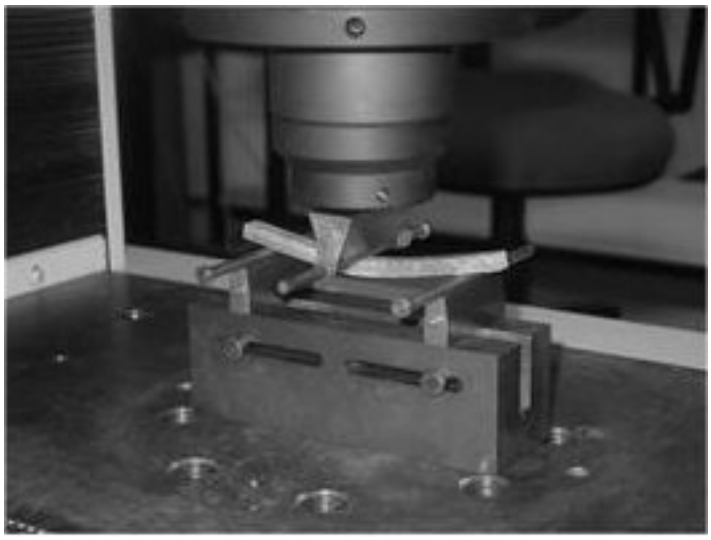

Figure 4.4. Photo of flexural test specimen under load.

### 4.6.2. Interlaminar Shear Properties

The apparent interlaminar shear strength of the composite specimens was determined performing short beam shear (SBS) tests according to ASTM method D2344-84. The SBS specimens 140 mm in length, 20 mm in depth and 20 mm in width were sectioned from the composite laminates. The length to thickness ratio and span to thickness ratio were kept constant at 7 and 5, respectively. The crosshead speed was remained constant at 1.3 mm/min, ten specimens from each set were tested using the universal test machine and load at break was recorded. Figure 4.5 shows the SBS test specimen under load. The apparent shear strength ($\tau_{max}$) was calculated based on;

$$\tau_{\max} = \frac{0.75P_B}{bd} \tag{4.5}$$

where $P$ is the breaking load, $b$ and $d$ are the width of the specimens and thickness of the specimen, respectively.

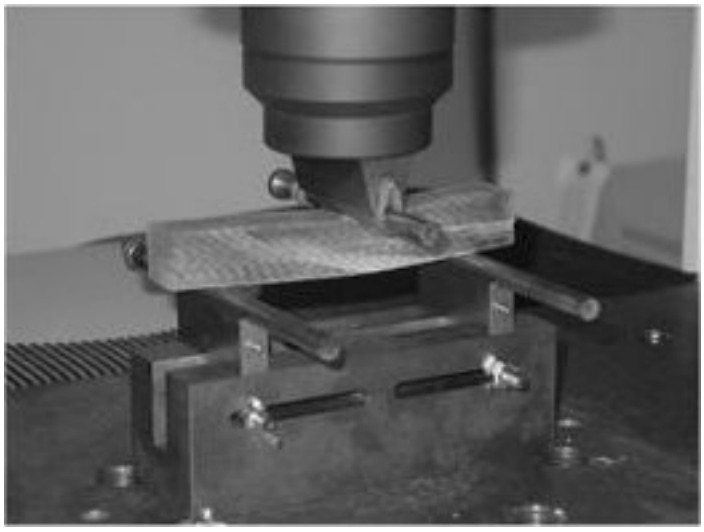

Figure 4.5. Photo of Short Beam Shear test specimen under load.

### 4.6.3. Compressive Properties

Compression test method according to ASTM D 695-M was used to measure the ply-lay up and in-plane compressive strength, modulus and strain to failure values of the composite panels. For this purpose, compression test specimens were sectioned from

larger RTM processed composite panels and tests along the mentioned directions were performed using the mechanical test machine at a crosshead speed of 1.3 mm/min. At least 10 specimens for each set were tested and force versus stroke values was recorded using a Shimadzu$^{TM}$ universal test machine. The compressive stress values were obtained by dividing load values with cross-sectional area of the specimens. The strain was estimated by dividing the adjusted (for machine compliance) stroke values with the initial specimen thickness. The yield stress values were estimated based on the transition values from linear to non-linear behavior. The modulus values were also estimated from the slope of the stress–strain graphs. Failure modes occurred within the specimen during the compressive loading was examined using SEM.

### 4.6.4. Fracture Toughness

Mode I Interlaminar fracture toughness of the composites was measured using SENB method, ASTM D 5045-91a. The SENB specimens were sectioned from composite laminates with the width of 10 mm, depth of 20 mm and length of 88 mm (Figure 4.6). In both geometries the crack length, $a$, were selected in the range of $0.45<a/W<0.55$, where $W$ is the depth of composite panel. The specimens were tested at crosshead speed of 10 mm/min. Mode I fracture toughness, $K_{ic}$, values were calculated using,

$$K_{ic} = \left(P_Q / BW^{1/2}\right) f(x) \tag{4.6}$$

where (0<x<1) and $S/W = 4$ :

$$f(x) = 6x^{1/2} \frac{\left[1.99 - x(1-x)\left(2.15 - 3.93x + 2.7x^2\right)\right]}{(1+2x)(1-x)^{3/2}}, \qquad x = a/W \tag{4.7}$$

where $P_Q$ is the applied load, $B$ is the specimen thickness, $S$ is the span length, $W$ is the specimen width, $a$ is the crack length.

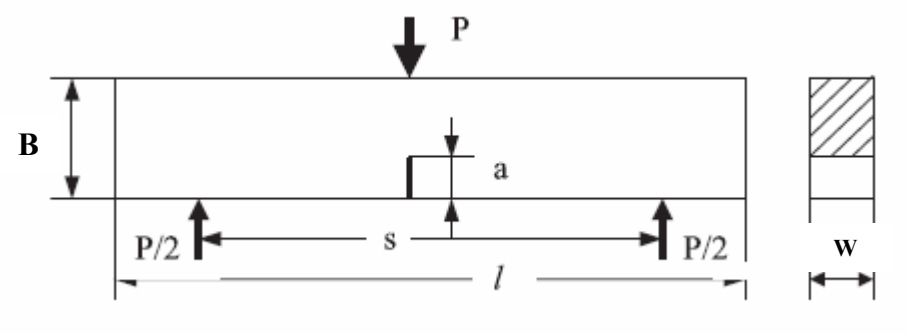


Figure 4.6. Sketch of single edge notch bend (SENB) test specimen.

## 4.7. Ballistic Testing

Ballistic testing on composite panels was conducted using 7.62 mm ball (B), 7.62 mm armor piercing (AP) and 7.62 mm fragment-simulating projectiles (FSPs). The laminate armor plates with and without alumina and aluminum tiles, were tested using a ballistic test facility, schematically shown in Figure 4.7. The striking velocities of the projectiles were measured using a chronograph. For the ballistic test, velocities of projectiles were set in the range of 420 to 1173 m/s.

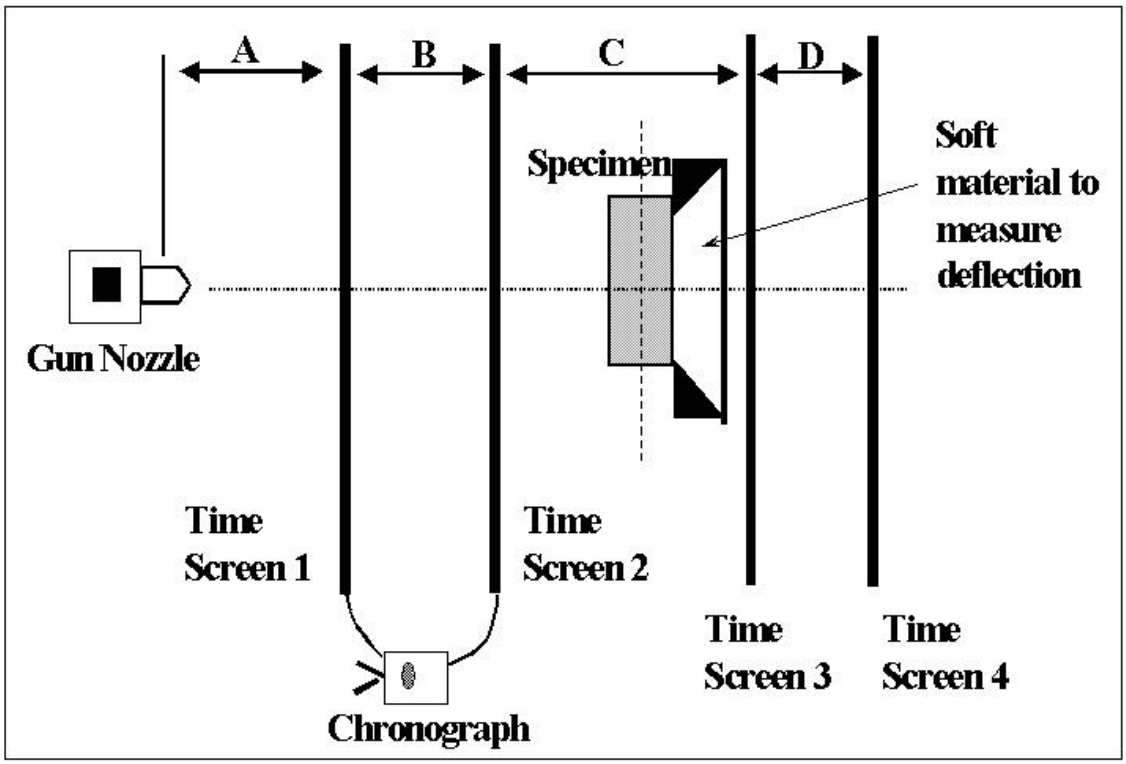


Figure 4.7. Schematic of ballistic test set up.

## 4.8. Evaluation of Damage Modes after Impact

The panels were examined after the ballistic test and size of visible ballistic damage was measured on the front and back surfaces of the panels. Also the panels were sectioned and the damage modes were examined.

# CHAPTER 5

## RESULTS AND DISCUSSION

In this chapter, the results of the investigation of the mechanical properties and ballistic performance of the E-glass polyester composites and also the ballistic performance of the sandwich structures with alumina and aluminum tiles are presented.

## 5.1. Composite Processing

A variety of E-glass reinforced polymer matrix composite panels were produced by RTM method. In this study, the composite panels made with E-glass $0^o/90^o$ woven fabrics and $0^o/90^o$ biaxial and $0^o/+45^o/-45^o/90^o$ quadraxial stitched non-crimp fabrics as reinforcing material were produced. Unsaturated polyester as matrix material was used to produce lightweight composites. Alumina tiles and aluminum plates were added to improve the ballistic performance of the composites. Figure 5.1 shows the photos of typical panels produced with RTM technique. Characteristics of the composite plates manufactured within the study are listed in Tables 5.1 and 5.2. In addition, ballistic panel number 14 was damaged in laboratory conditions and it is not listed in Table 5.1.

The fiber volume fractions of the produced composites were measured by burn-out technique. The average fiber volume fraction obtained from the samples of the composite panels were calculated to be about 50.75 (±2.06) % for the polymer composites made with 50 plies. The fiber volume fraction were calculated for the composites made with $0^o/90^o$ biaxial and $0^o/+45^o/-45^o/90^o$ quadraxial stitched non-crimp fabrics and fiber volume fractions were 52.03 (±1.85) % and 50.64 (±2.04) %, respectively.

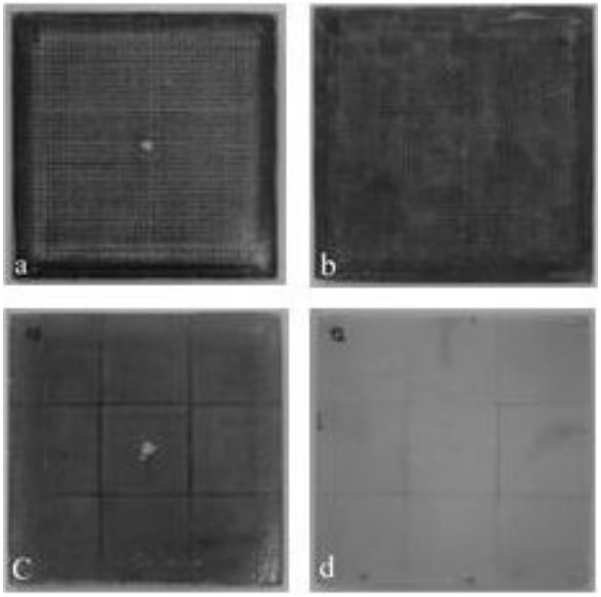


Figure 5.1. Photos of the typical composite structures manufactured by RTM. Characteristics of the specimens are listed in Table 5.1. Panel numbers are a) 1, b) 8, c) 10, d) 12.

Table 5.1. Composite panels fabricated with woven fabrics by RTM process for ballistic testing.

| Ballistic Panel Number | Sandwich Structure | Thickness (mm) | Ceramic (metal) thickness / composite thickness ratio ($h_1/h_2$) | Panel weight (kg) | Areal density ($kg/m^2$) |
|---|---|---|---|---|---|
| 1* | $C_{30ply}$ | 20 | - | 3.360 | 37.33 |
| 2 | $C_{50ply}$ | 20 | - | 3.180 | 35.33 |
| 3* | $C_{32ply}$ | 20 | - | 3.514 | 39.04 |
| 4 | $C_{50ply}$ | 20 | - | 3.174 | 35.26 |
| 5 | $C_{50ply}$ | 20 | - | 3.192 | 35.46 |
| 6 | $C_{52ply}$ | 20 | - | 3.240 | 36 |
| 7 | $C_{50ply}$ | 20 | - | 3.296 | 36.62 |
| 8 | $C_{50ply}$ | 20 | - | 3.098 | 34.42 |
| 9 | $C_{50ply}$ | 20 | - | 3.154 | 35.04 |
| 10 | $C_{4ply}/Al/C_{22ply}$ | 20(3/10/7) | 1 | 4.100 | 45.55 |
| 11 | $C_{3ply}/Al/C_{19ply}$ | 20 (3/10/7) | 1 | 4.049 | 44.98 |
| 12 | $C_{4ply}/Al_2O_3/C_{18ply}$ | 22 (2/13/7) | 1.857 | 5.617 | 62.41 |
| 13 | $C_{4ply}/Al_2O_3/C_{18ply}$ | 22 (2/13/7) | 1.857 | 5.635 | 62.61 |
| 15 | $C_{10ply}/Al_2O_3/C_{50ply}$ | 48 (4/25/19) | 1.041 | 11.640 | 129.33 |

C: Composite. * Fabric density 800 $g/m^2$, all the other panels are made with glass fabric density of 500 $g/m^2$. Panel dimensions 300x300 mm

Table 5.2. Composite panels fabricated with stitched non-crimp fabrics by RTM process.

| Panel Number | Structure | Thickness (mm) | Panel Weight (kg) | Areal Density ($kg/m^2$) |
|---|---|---|---|---|
| 1 | $C\text{-}1_{27ply\text{-}Herkon}$ | 20 | 3.460 | 38.44 |
| 2 | $C\text{-}1_{27ply\text{-}Camelyaf266}$ | 20 | 3.456 | 38.40 |
| 3 | $C\text{-}2_{12ply\text{-}Herkon}$ | 20 | 3.420 | 38.00 |
| 4 | $C\text{-}2_{12ply\text{-}Camelyaf\,266}$ | 20 | 3.380 | 37.55 |
| 5 | $C\text{-}2_{12ply\text{-}Herkon}$ | 20 | 3.360 | 37.33 |

C-1: $0^o/90^o$ biaxial stitched non-crimp fabrics, C-2 : $0^o/+45^o/-45^o/90^o$ quadraxial stitched non-crimp fabrics.

## 5.2. Mechanical Properties of Composites

### 5.2.1. Flexural Strength and Modulus

The flexural stress in the outer fiber vs. strain in the outer fiber was plotted in the Figures 5.2-5.5. The maximum stress in the outer fiber occurs at the mid span, when the composite sample beam supported at two points and loaded at mid point. Figure 5.2 shows flexural stress vs. strain response of E-glass/polyester composites ($0^o/90^o$ woven fabric/ isophthalic polyester). The stress-strain response of the composite is nearly linear at the beginning but changes to non-linear behaviour at the later stage of deformation. The flexural strength and flexural modulus values were measured and the average values were found to be 624±83 MPa and 17±0.23 GPa, respectively for $0^o/90^o$ woven fabrics. It was obtained that the flexural strength and modulus values of the composites produced with biaxial and quadraxial non-crimp fabrics were different from those of composites produced with woven fabrics. So, it was concluded that the fiber type used as reinforcement material has the same effects on the flexural strength of the composite. As seen in Figures 5.3, 5.4, and 5.5, the flexural strength and flexural modulus of composites produced with non-crimp fabrics are lower than these of composites produced with woven fabrics. The average flexural strength and flexural modulus of composites fabricated with the $0^o/+45^o/-45^o/90^o$ quadraxial non-crimp fabrics and orthophthalic polyester were measured as 527±53 MPa and 13±2 GPa,

respectively (Figure 5.3). The average value of flexural strength and flexural modulus of composites that containing $0^o/+45^o/-45^o/90^o$ quadraxial non-crimp fabrics and isophthalic polyester, were measured 511±52 MPa and 12±0.6 GPa, respectively (Figure 5.4). Also, it was clearly seen that the composite structure made with $0^o/90^o$ biaxial stitched fabrics and orthophthalic polyester has better flexural strength and modulus values than the structure contains $0^o/+45^o/-45^o/90^o$ quadraxial stitched non-crimp fabrics. The average values of flexural strength and modulus for this structure were measured as 576±89 and 16±1.1 GPa, respectively (Figure 5.5). The flexural strengths are also higher than or similar to their compressive strengths. All the laminates tested along a fiber direction show a brittle failure, generally by outer ply delamination on a tensile surface. The delamination zone starts at the middle of the specimen where the bending moment is maximum, then propagates outwards until significant fiber rupture occurs at the middle section on the tensile surface. This typical failure mode can be observed in all types of composites produced and tested in this study. Delamination along the fiber strands can be observed on both the tensile surface and the compressive surface. Large deflection is reached before the final failure with fiber rupture occurs. In the literature, the similar test results were obtained (Wang 2002).

Table 5.3. The flexural properties of composite plates.

| Specimen | Flexural Strength (MPa) | Flexural Modulus (GPa) |
|---|---|---|
| $0^o/90^o$ woven E-glass fabrics - C266 | 624 ± 83 | 17 ± 0.23 |
| $0^o/45^o/+45^o/90^o$ quadraxial non-crimp fabrics, Herkon | 527 ± 53 | 13 ± 2 |
| $0^o/45^o/+45^o/90^o$ quadraxial non-crimp fabrics, C266 | 511 ± 52 | 12 ± 0.6 |
| $0^o/90^o$ biaxial non-crimp fabrics, Herkon | 576 ± 89 | 16 ± 1.1 |

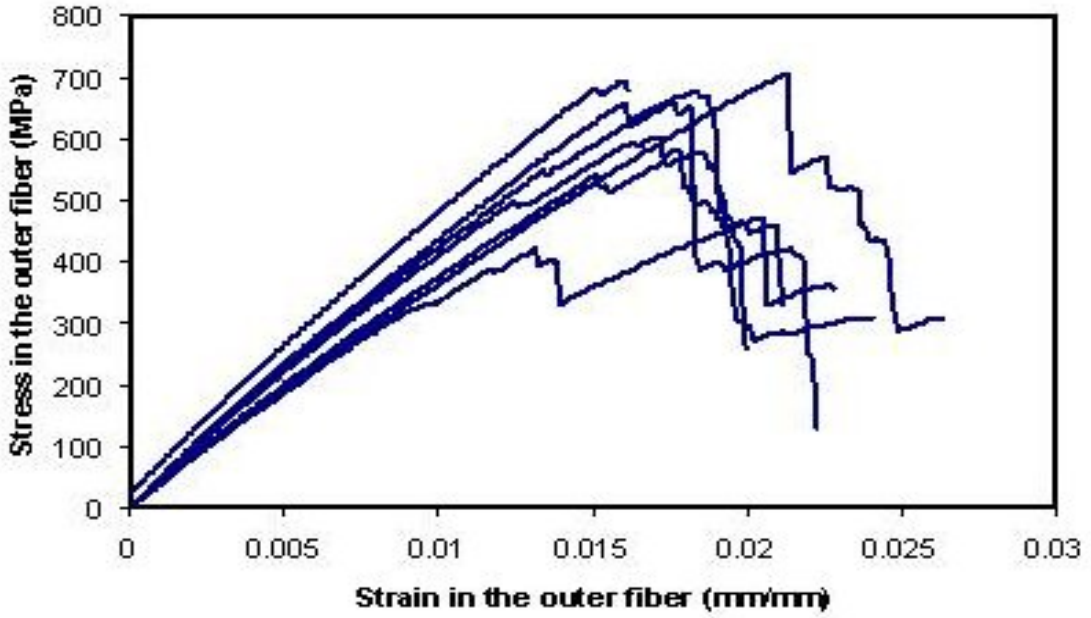


Figure 5.2. Flexural stress vs. strain graphs of the E-glass/polyester composites ($0^o/90^o$ woven fabrics, Camelyaf 266 isophthalic polyester).

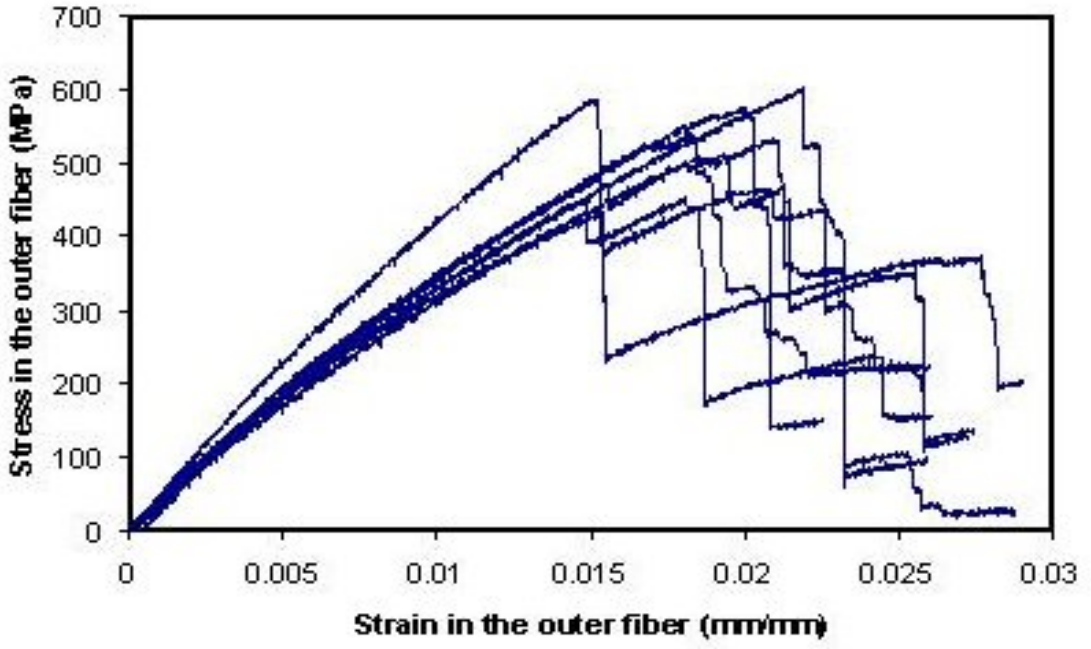


Figure 5.3. Flexural stress vs. strain graphs of the E-glass/polyester composites ($0^o/-45^o/+45^o/90^o$ quadraxial non-crimp stitched fabrics, Herkon orthophthalic polyester).

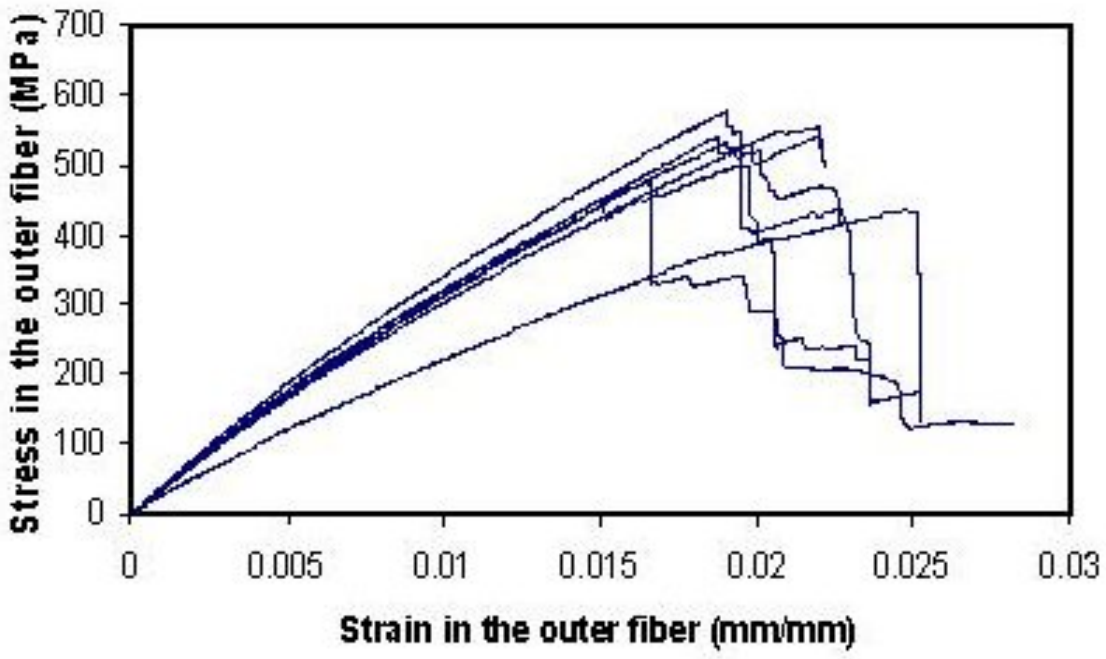


Figure 5.4. Flexural stress vs. strain graphs of the E-glass/polyester composites ($0^o$/-$45^o$/+$45^o$/$90^o$ quadraxial stitched non-crimp fabrics, Camelyaf 266 isophthalic polyester)

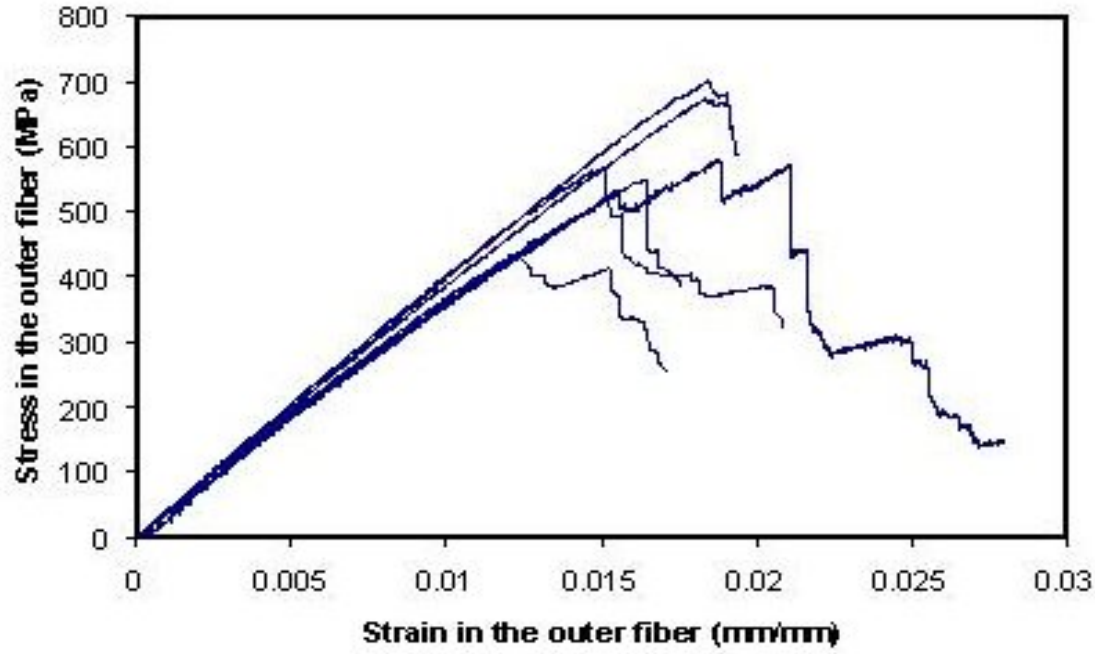


Figure 5.5. Flexural stress vs. strain graphs of the E-glass/polyester composites ($0^o$/$90^o$ biaxial stitched non-crimp stitched fabrics, Herkon orthophthalic polyester)

## 5.2.2. Interlaminar Shear Strength

The apparent interlaminar shear strength of E-glass / polyester composites was determined performing SBS test. As an example the apparent shear strength for woven fabrics and isophthalic polyester was measured as 30±4 MPa. The apparent shear strength values for the other composite structures are presented in the Figure 5.6. It was observed that typical failure mode, in the short beam test was the beam delamination of the plies.

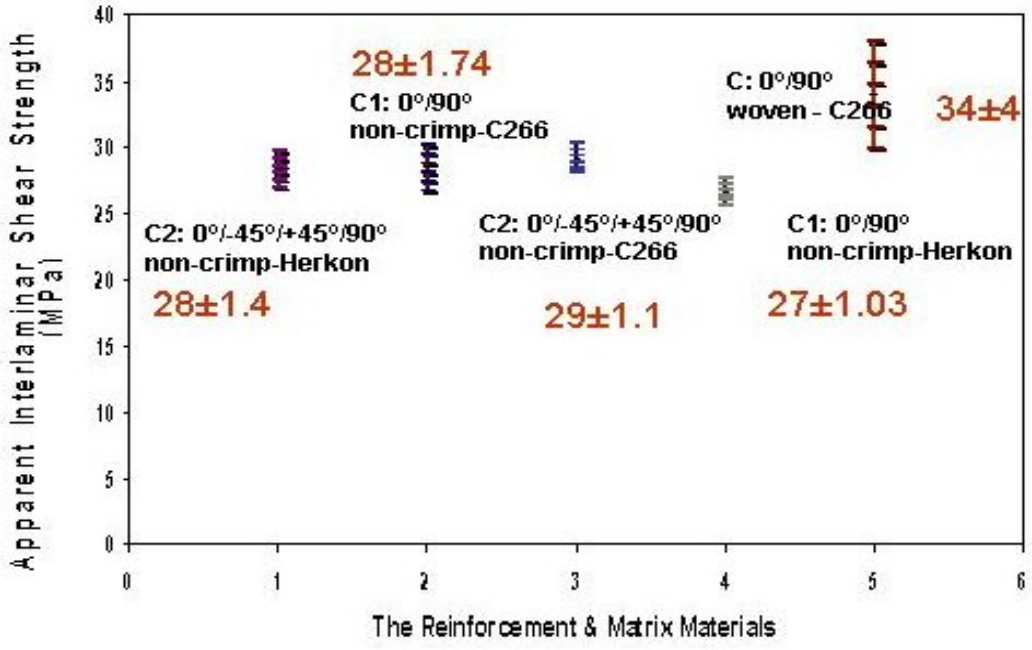


Figure 5.6. The apparent interlaminar shear strength of E-glass polyester composites with different reinforcement and matrix material ($0^o/90^o$ woven, $0^o/90^o$ biaxial, $0^o/-45^o/+45^o/90^o$ quadraxial stitched non-crimp fabrics were used with isophthalic (C266) and orthophthalic (Herkon) polyester resins were used.

## 5.2.3. Interlaminar Fracture Toughness

Mode I plane strain fracture toughness of the composite specimens were measured using SENB specimens. Figure 5.7 shows the SENB test specimens loaded in-plane and ply-lay up directions. Table 5.4 shows the $K_{ic}$ values for the E-

glass/polyester composites measured from SENB samples loaded in ply-lay up and in-plane directions.

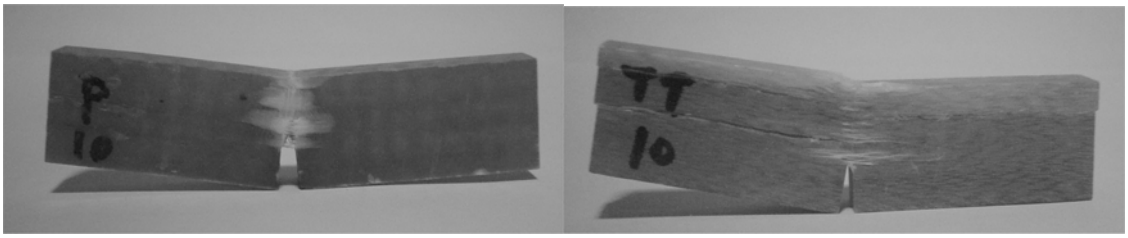


Figure 5.7. SENB test specimens loaded (a) in-plane direction, (b) ply-lay up direction.

Table 5.4. $K_{ic}$ values of the E-glass/polyester composites measured from SENB samples

| Specimen | $K_{ic}$ (MPa $m^{1/2}$) Ply-lay up direction | $K_{ic}$ (MPa $m^{1/2}$) In-plane direction |
|---|---|---|
| $0^o/90^o$ woven E-glass fabrics - C266 | 1.23 ± 0.09 | 1.49 ± 0.07 |
| $0^o/45^o/+45^o/90^o$ quadraxial non-crimp fabrics, Herkon | 0.921 ± 0.083 | --- |
| $0^o/45^o/+45^o/90^o$ quadraxial non-crimp fabrics, C266 | 0.715 ± 0.165 | 1.830 ± 0.148 |
| $0^o/90^o$ biaxial non-crimp fabrics, C266 | 1.196 ± 0.160 | --- |
| $0^o/90^o$ biaxial non-crimp fabrics, Herkon | 0.875 ± 0.252 | 1.601 ± 0.229 |

C266: Isopthalic polyester resin, Herkon: orthophthalic polyester resin

## 5.2.4. Compression Stress-Strain Behaviour

Figures 5.8 and 5.9 show compressive stress vs. strain response of woven E-glass/polyester composites loaded along the ply-lay up and in-plane directions, respectively. For ply-lay up direction, fracture occurs at about the ultimate stress level. The stress-strain behavior of the composites loaded along the in-plane direction differs from the ply-lay up direction. Those samples show pre cracking following a linear

initial portion of the curves. At the pre-cracking stress, local interlaminar fracture occurs.

The test results showed that the average strength values are 532±38 MPa and 295±88 MPa for ply-lay up and in-plane directions, respectively. Also, the average compressive modulus values measured from the initial part of the graphs are 4.49±0.15 GPa and 5.42±1.5 GPa for ply-lay up and in-plane directions, respectively. The compressive strength and modulus values of composites produced with various types of reinforcements and polyester are summarized in Table 5.5. Also, the compressive stress-strain behaviour of the listed composites are shown in Figures 5.10 – to 5.15.

Table 5.5. The compressive strength and modulus values of composites made with various fabrics and polyesters.

| Specimen | In plane direction | | Ply-lay up direction | |
|---|---|---|---|---|
| | Compressive Strength (MPa) | Compressive Modulus (GPa) | Compressive Strength (MPa) | Compressive Modulus (GPa) |
| $0^o/90^o$ woven – C266 | 295 ± 88 | 5.42 ± 1.5 | 532 ± 38 | 4.49 ± 0.15 |
| $0^o/-45^o/+45^o/90^o$ quadraxial – C266 | 268 ± 18 | 5.22 ± 0.2 | 482 ± 19 | 3.3 ± 0.1 |
| $0^o/-45^o/+45^o/90^o$ quadraxial– Herkon | 275 ± 54 | 5.3 ± 1 | 531 ± 37 | 3.6 ± 0.2 |
| $0^o/90^o$ biaxial – Herkon | 266 ± 30 | 5.9 ± 0.7 | 506 ± 26 | 3.9 ± 0.2 |

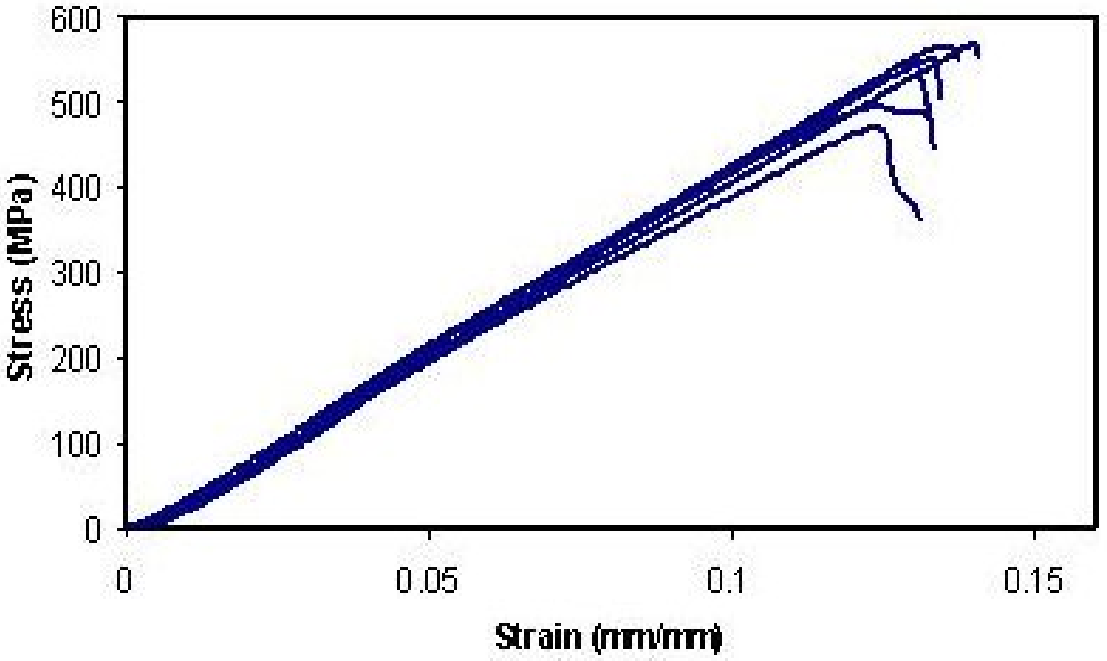


Figure 5.8. Compressive stress vs. strain graphs of the RTM fabricated E-glass/polyester composites (Loaded along the ply-lay up direction; $0^o/90^o$ woven fabrics, Camelyaf 266 isophthalic polyester).

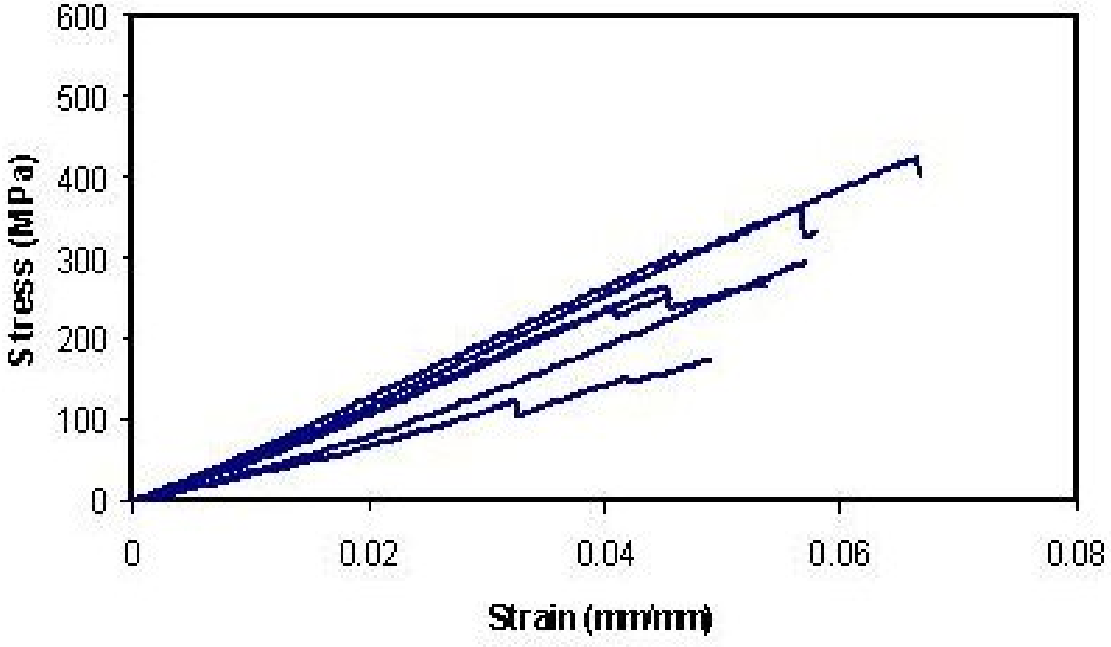


Figure 5.9. Compressive stress vs. strain graphs of the RTM fabricated E-glass/polyester composites (Loaded along the in-plane direction; $0^o/90^o$ woven fabrics, Camelyaf 266 isophthalic polyester).

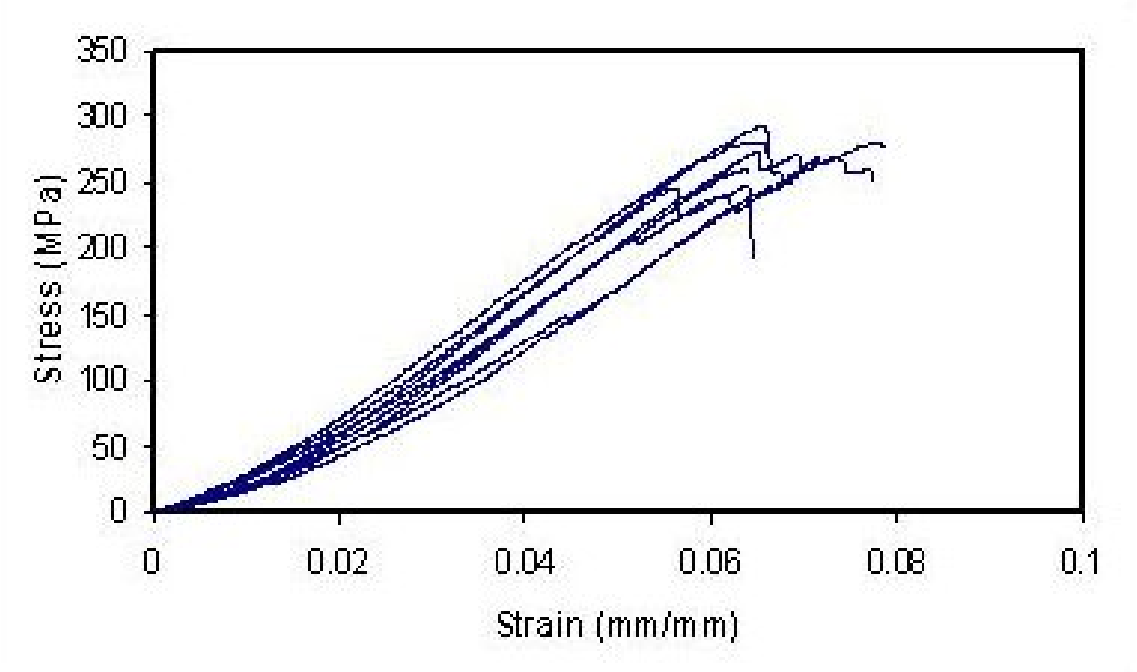


Figure 5.10. Compressive stress vs. strain graphs of the RTM fabricated E-glass/polyester composites (Loaded along the in-plane direction; $0^o$/-$45^o$/+$45^o$/$90^o$ quadraxial non-crimp fabrics, Camelyaf 266 isophthalic polyester).

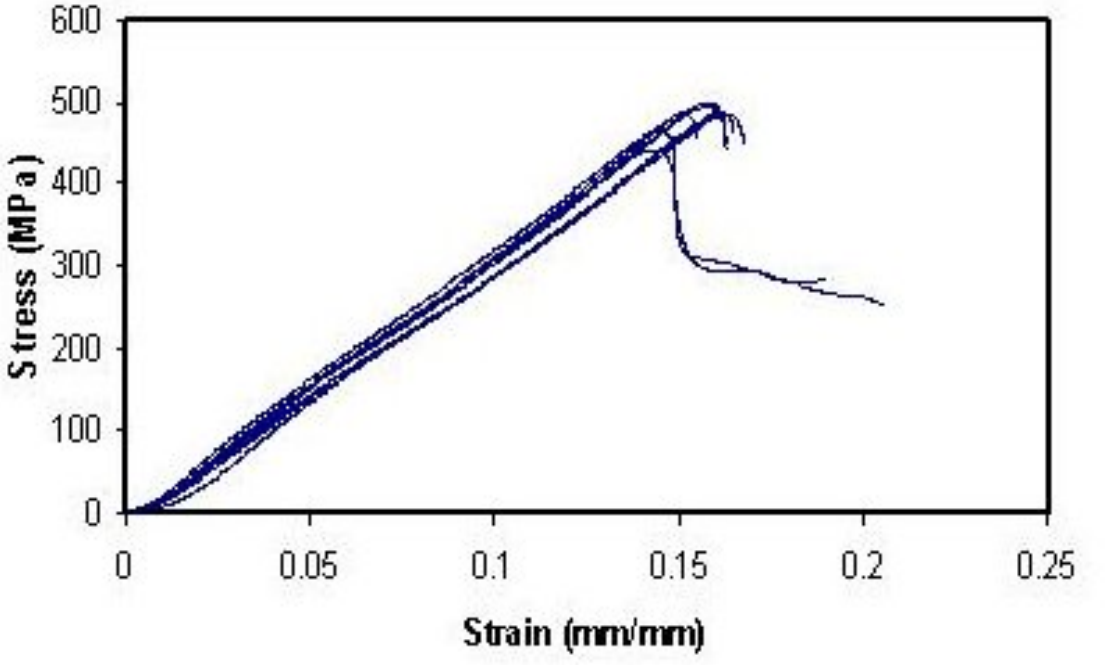


Figure 5.11. Compressive stress vs. strain graphs of the RTM fabricated E-glass/polyester composites (Loaded along the ply lay up direction; $0^o$/-$45^o$/+$45^o$/$90^o$ quadraxial non-crimp fabrics, Camelyaf 266 isophthalic polyester).

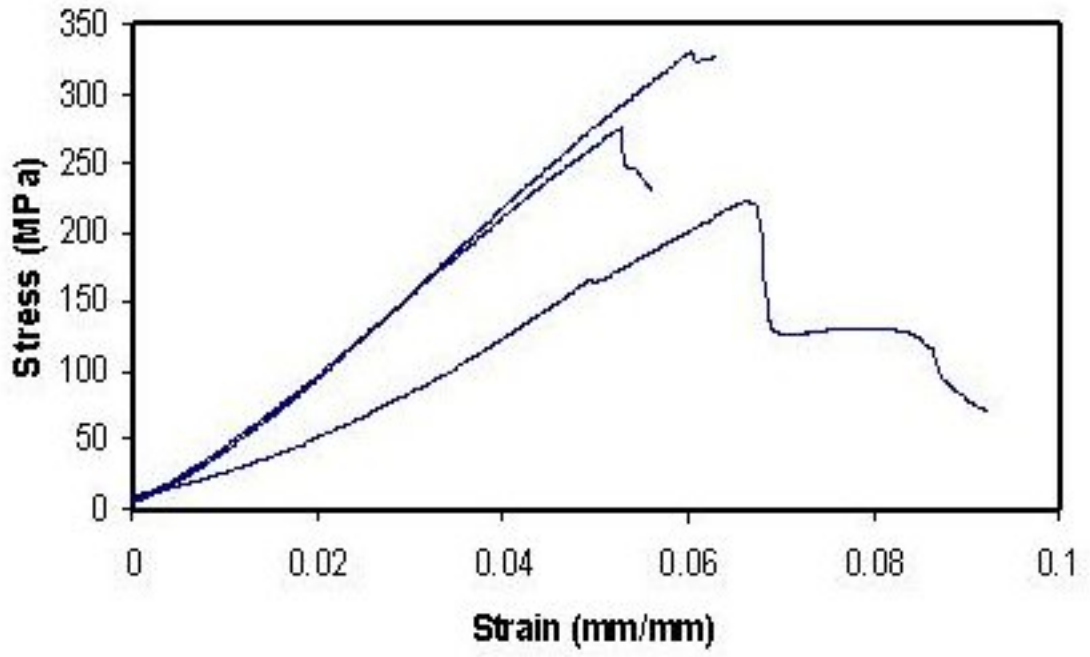


Figure 5.12. Compressive stress vs. strain graphs of the RTM fabricated E-glass/polyester composites (Loaded along the in-plane direction; $0^o$/-$45^o$/+$45^o$/$90^o$ quadraxial non-crimp fabrics, Herkon orthophthalic polyester).

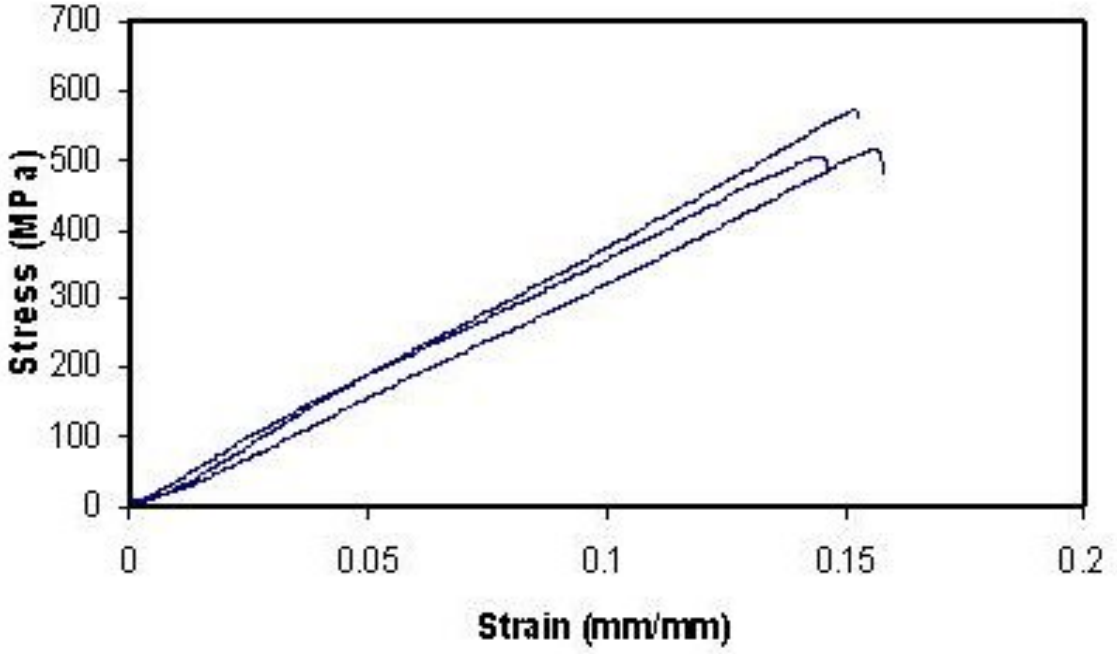


Figure 5.13. Compressive stress vs. strain graphs of the RTM fabricated E-glass/polyester composites (Loaded along the ply lay up direction; $0^o$/-$45^o$/+$45^o$/$90^o$ quadraxial non-crimp fabrics, Herkon orthophthalic polyester).

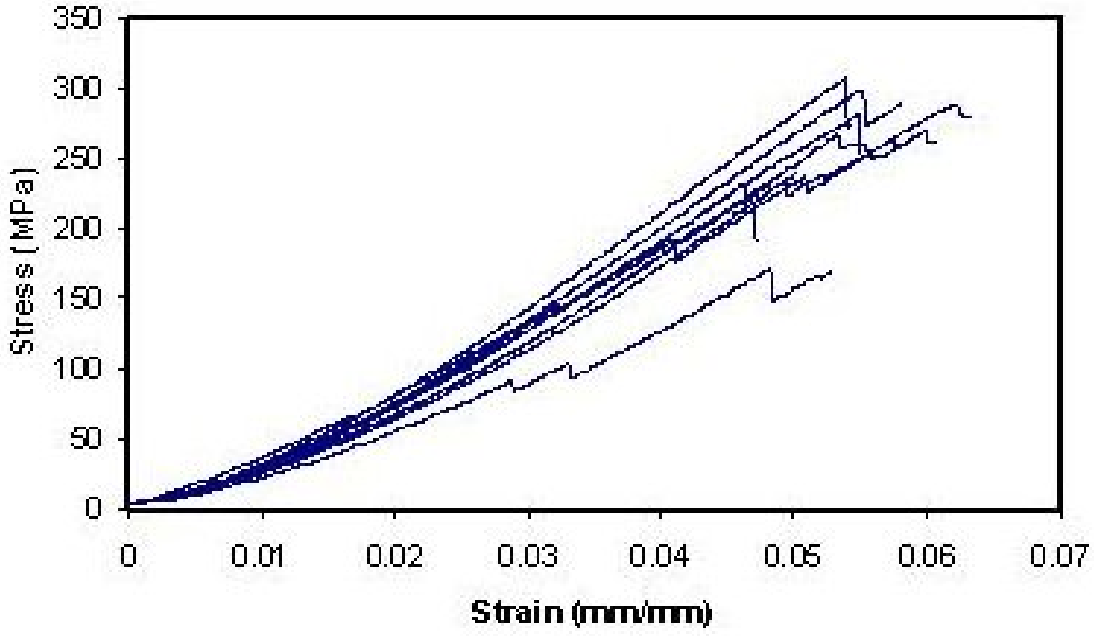


Figure 5.14. Compressive stress vs. strain graphs of the RTM fabricated E-glass/polyester composites (Loaded along the in plane direction; $0^o/90^o$ biaxial stitched fabrics, Herkon orthophthalic polyester).

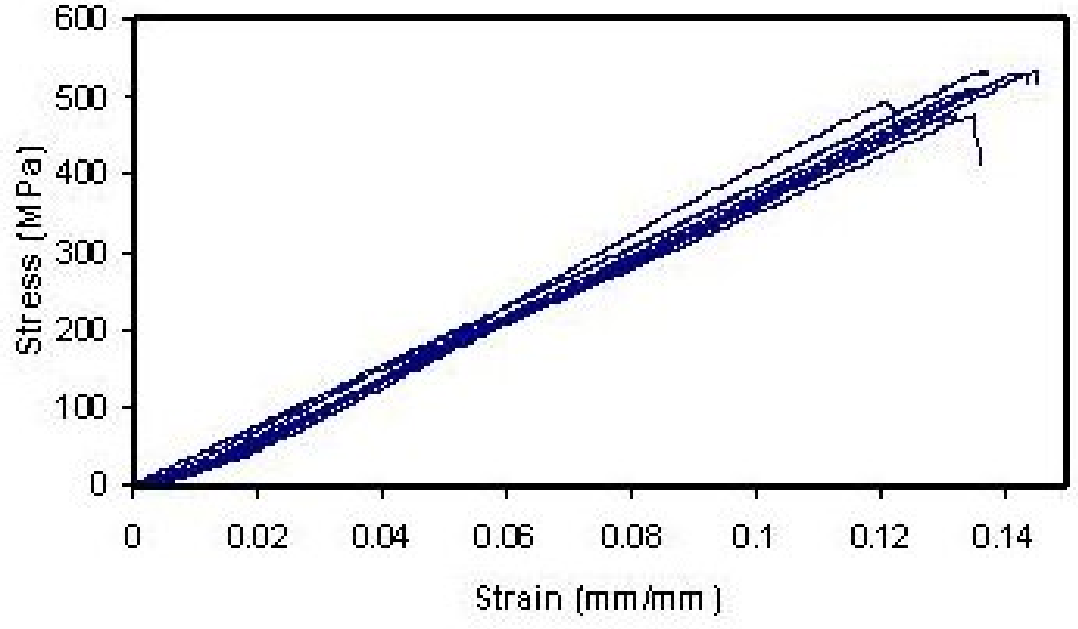


Figure 5.15. Compressive stress vs. strain graphs of the RTM fabricated E-glass/polyester composites (Loaded along the ply lay up direction; $0^o/90^o$ biaxial stitched fabrics, Herkon orthophthalic polyester).

## 5.3. Fracture Mechanisms

Photographs of the failed samples tested (woven fabrics/ isophthalic polyester) in in-plane and through thickness (ply-lay up) directions are shown in Figure 5.16. Failure in the in-plane direction occurred at nearly 45 degrees to the loading axis. In the through thickness direction failure occurred similarly at 45 degrees to the loading direction for the samples.

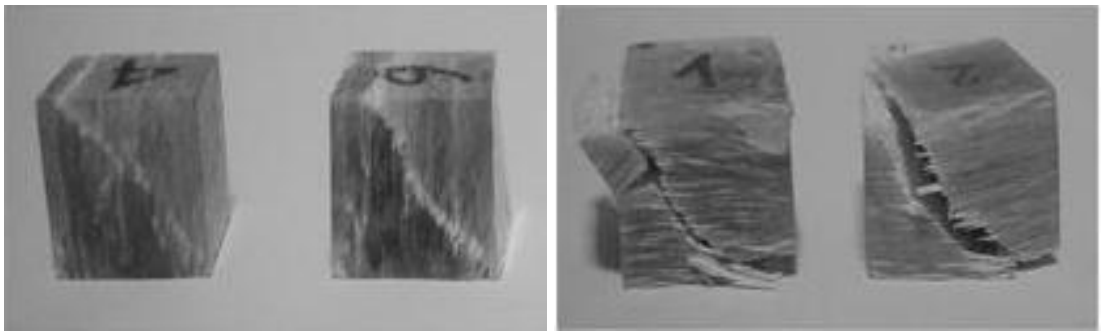

Figure 5.16. Photographs of failed samples tested in a) in-plane direction, b) ply-lay up direction

Microscopic observations clearly showed that axial splitting and king banding were the main failure mechanism in samples loaded along in-plane direction (Figure 5.17 a). Also fiber buckling was observed in the same specimens and shown in Figures 5.17 b.

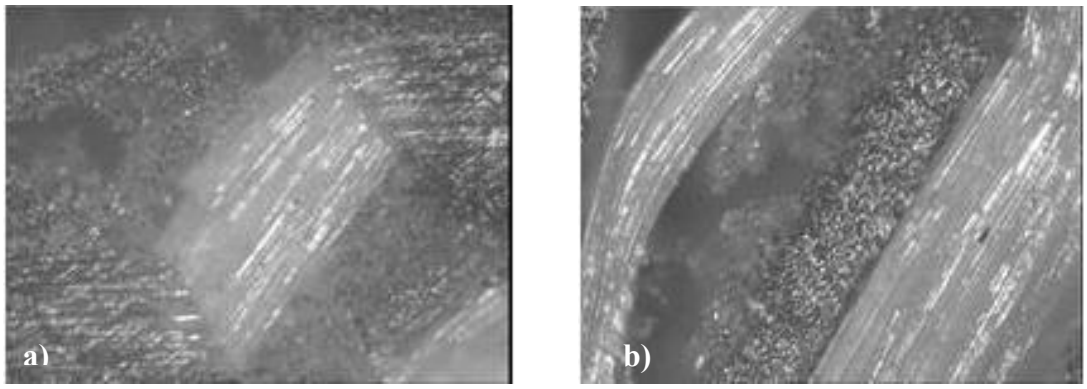


Figure 5.17. Optical micrographs from the E-glass/polyester composite loaded in in-plane direction. a) king banding, b) fiber buckling.

Figure 5.18 and Figure 5.19 show the fracture surface SEM micrographs of the compression test specimens loaded along in-plane direction. As seen in these figures, matrix cracking and fiber matrix debonding and also fiber fractures occured due to the loadings.

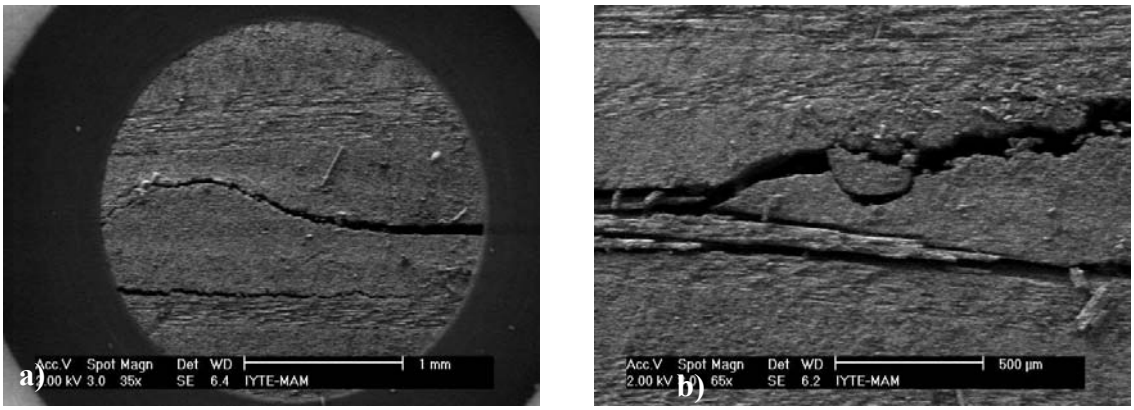


Figure 5.18. SEM micrographs of sample tested in in-plane direction showing, a) matrix cracking b) fiber matrix debonding

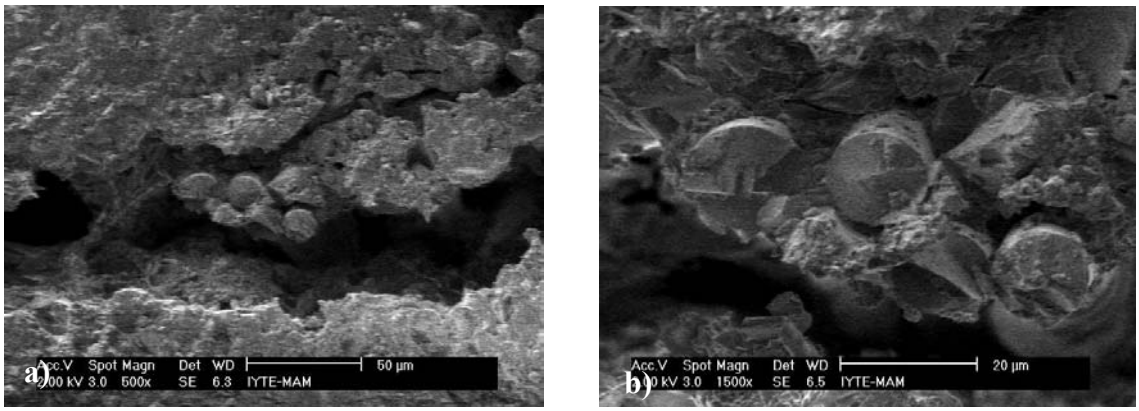


Figure 5.19. SEM micrographs of sample tested in in-plane direction showing, a) fiber matrix debonding b) fiber fracture.

Figure 5.20 shows the fracture surface SEM micrographs of the compression test specimens loaded along ply-lay up direction. As seen in these figures, matrix and fiber fractures, as well fiber matrix debondings were observed

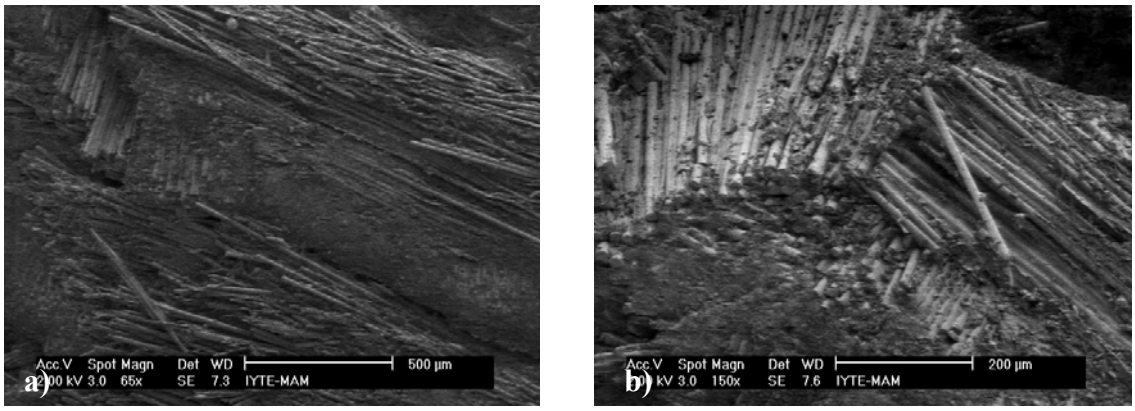


Figure 5.20. SEM micrographs of sample tested in ply-lay up direction showing, a) fiber and matrix fracture, b) fiber debonding.

## 5.4. Ballistic Properties of Fiber Reinforced Polymer Composite Materials

Ballistic performance results of the composite panels impacted with three different types of projectiles at various velocities is summarized in Table 5.6. Ballistic test results showed that the composite panels without any additional ceramic or metallic layer have ballistic resistance against 7.62 mm FSP projectiles up to 1001 m/s velocities. So, all of these panels stopped the 7.62 mm FSP at test velocities in the range of 435 to 1001 m/s with only partial penetration. Above 1001 m/s, perforations of the composites were observed. Figure 5.21 and Figure 5.22 show the damages on the front and back face of the panels subjected to impact by FSPs, respectively. In the case that the same composite panels were subjected to ballistic impact by armor piercing projectiles (AP), full penetration of the AP projectiles (perforation) were observed at all velocities (420 to 931 m/s) tested within the study. So, it can be concluded that the polymer composites fabricated in the study without any support layer are not sufficient to stop AP projectiles. The front and back face of the composite panels subjected to the AP projectiles at various velocities are shown in Figure 5.23.

Table 5.6. Ballistic performance results of composite armor panels impacted with different types of projectiles at various velocities. (AP: Armor-piercing projectile, FSP: Fragment simulating projectile, B: Ball projectile)

| Panel Number | Shoot Number | Projectile | Projectile Velocity [m/s] | Result |
|---|---|---|---|---|
| 2 | 1 | 7.62 FSP | 435 | PP |
| | 2 | 7.62 FSP | 548 | PP |
| 3 | 1 | 7.62 FSP | 826 | PP |
| | 2 | 7.62 FSP | 1015 | PE |
| 5 | 1 | 7.62 FSP | 831 | PP |
| | 2 | 7.62 FSP | 800 | PP |
| | 3 | 7.62 FSP | 696 | PP |
| 6 | 1 | 7.62 AP | 592 | PE |
| | 2 | 7.62 AP | 420 | PE |
| | 3 | 7.62 AP | 833 | PE |
| | 4 | 7.62 AP | 931 | PE |
| 8 | 1 | 7.62 FSP | 813 | PP |
| | 2 | 7.62 FSP | 794 | PP |
| | 3 | 7.62 FSP | 1119 | PE |
| 9 | 1 | 7.62 FSP | 1001 | PE |
| | 2 | 7.62 FSP | 1074 | PE |
| 11 | 1 | 7.62 AP | 441 | PE |
| | 2 | 7.62 B | 490 | PE |
| | 3 | 7.62 FSP | 861 | PP |
| | 4 | 7.62 FSP | 1090 | PE |
| | 5 | 7.62 B | 485 | PE |
| 12 | 1 | 7.62 AP | 928 | PP |
| | 2 | 7.62 AP | 594 | PP |
| | 3 | 7.62 AP | 446 | PP |
| 13 | 1 | 7.62 AP | 883 | PP |
| | 2 | 7.62 AP | 1007 | PP |
| 15 | 1 | 7.62 AP | 1020 | PP |
| | 2 | 7.62 FSP | 1173 | PP |

PP: Partial penetration, PE: Perforation

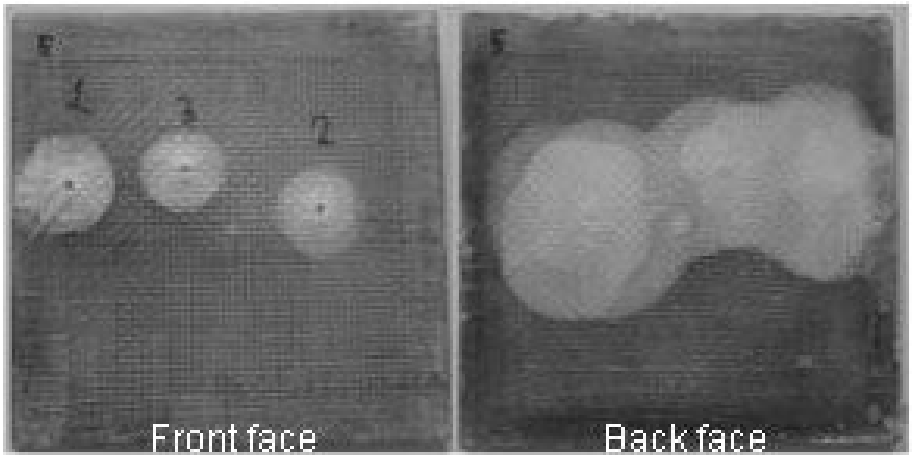


Figure 5.21. E-glass fiber/polyester composite panel subjected to ballistic impact with FSP projectiles (Panel number 5, velocities; 1. 831 m/s, 2. 800 m/s, 3. 696 m/s)

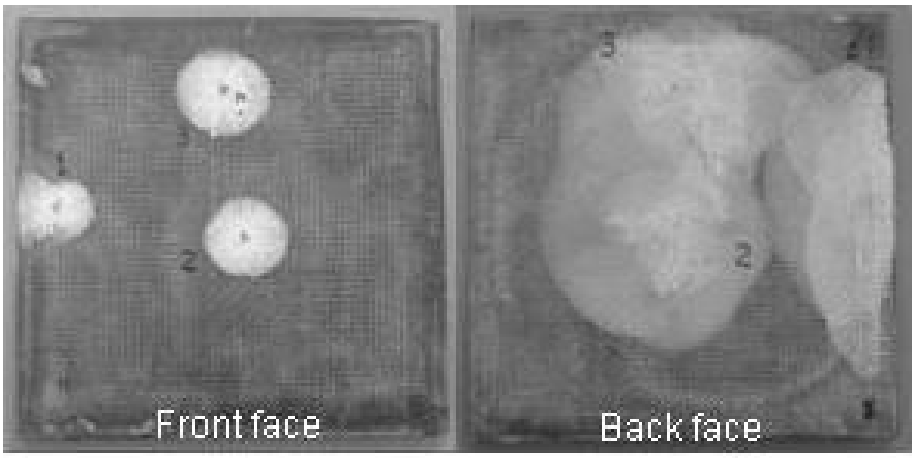


Figure 5.22. E-glass fiber/polyester composite panel subjected to ballistic impact with FSP projectiles (Panel number 8, velocities; 1. 813 m/s, 2. 794 m/s, 3. 1119 m/s)

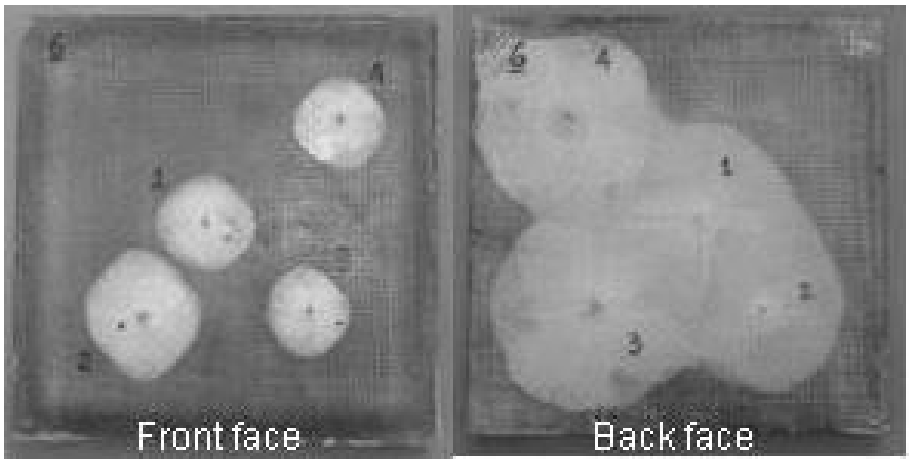


Figure 5.23. E-glass fiber/polyester composite panel subjected to ballistic impact with AP projectiles (Panel number 6, velocities; 1. 592 m/s, 2. 420 m/s, 3. 833 m/s, 4. 931 m/s)

On the other hand, the panels that are supported by ceramic tiles exhibited a better ballistic performance. The sandwich panels containing ceramic tiles subjected to the ballistic impact by AP and FSP projectiles exhibited only partial penetrations at all the velocities tested within the study (446-1020 m/s with AP and 1173 m/s with FSP, Figure 5.24 and Figure 5.25). For the composites supported by Al panels, perforation was observed with AP and ball projectiles even at low velocities (441m/s for AP and 485-490 m/s for Ball). In the case of FSPs, although perforation was observed at 1090 m/s, at lower velocity (861 m/s) partial penetration was occurred in Al/polymer composites (Figure 5.26). The results revealed that the addition of Al plates has no significant contribution to the ballistic resistance of polymer composites. On the other hand, incorporation of $Al_2O_3$ tiles significantly improves the ballistic resistance of the woven glass fabric reinforced polymer composites against AP and FSPs.

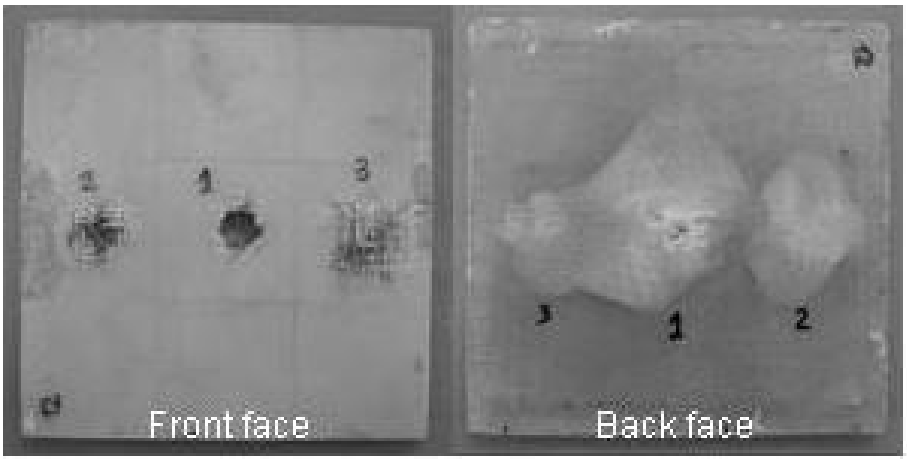


Figure 5.24. Alumina ($Al_2O_3$)/polymer composite panel subjected to ballistic impact with AP projectiles (Panel number 12, velocities; 1. 928 m/s, 2. 594 m/s, 3. 446 m/s)

To reveal the effect of fabric density, an additional panel with 800 g/m$^2$ fabrics was also fabricated. Figure 5.27 shows the ballistic test results of the multilayered composites. For this panel, perforation at 1015 m/s and partial penetration at 826 m/s was observed with FSP projectiles. The response is almost similar with those made with 500 g/m$^2$ fabrics. It was concluded that there is no significant effect of fabric density on the response of composites.

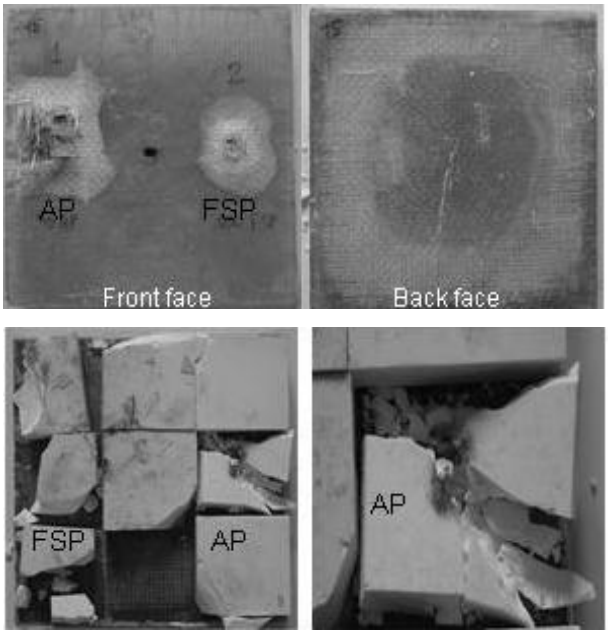


Figure 5.25. Alumina ($Al_2O_3$)/polymer composite panel subjected to ballistic impact with AP projectiles (Panel number 15, velocities; 1. 1020 m/s, 2. 1173 m/s)

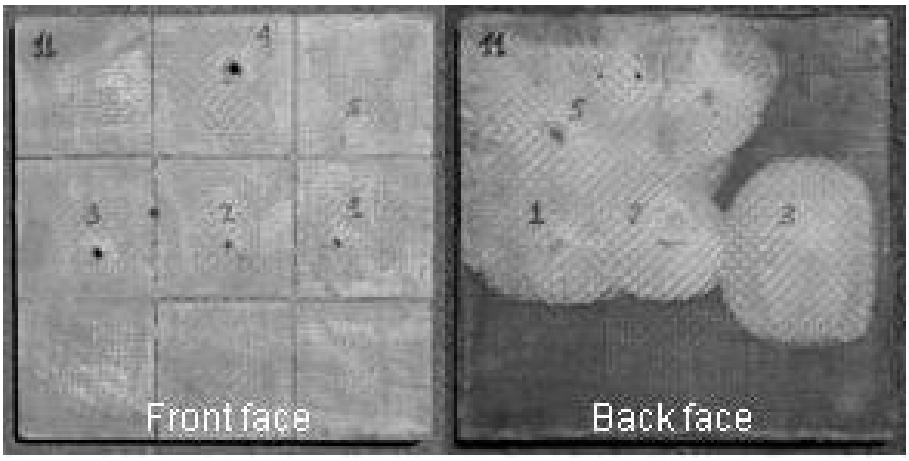


Figure 5.26. Aluminum (Al)/polymer composite panel subjected to ballistic impact with different projectiles. (Panel number 11, velocities; 1.(AP) 441 m/s, 2.(B) 490 m/s, 3.(FSP) 861 m/s, 4.(FSP) 1090 m/s, 5. (B) 485m/s)

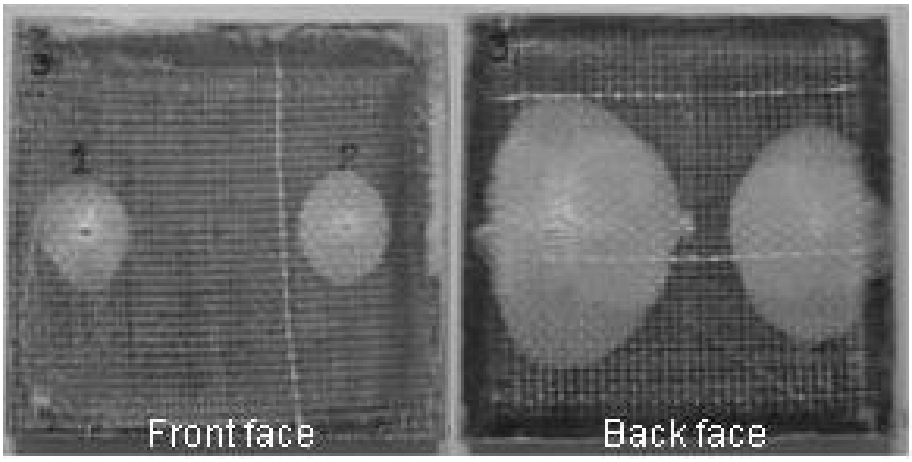


Figure 5.27. E-glass fiber/polyester composite panel subjected to ballistic impact with FSP projectiles (Panel number 3, velocities; 1. 826 m/s, 2. 1015 m/s)

## 5.5. Ballistic Damage within the Composite Armor

Figure 5.30 is an example showing the cross section of the polymer composites after ballistic impact. As it can be seen, a conical shaped damage zone occurred within the panels. This damage geometry is typical observed within composites and reported in the literature (Gellert *et al.* 2000) extensively (figure 5.28 and 5.29). Table 5.6 is also exhibiting the damage extension within the panels. As the velocity of the FSP is

increasing, the delamination at the back face increases although the amount of the damage remains almost constant at the front face. This may be due to the wave cancellation at the entrance face, but increased interlaminar fracture within the zones close to the back face.

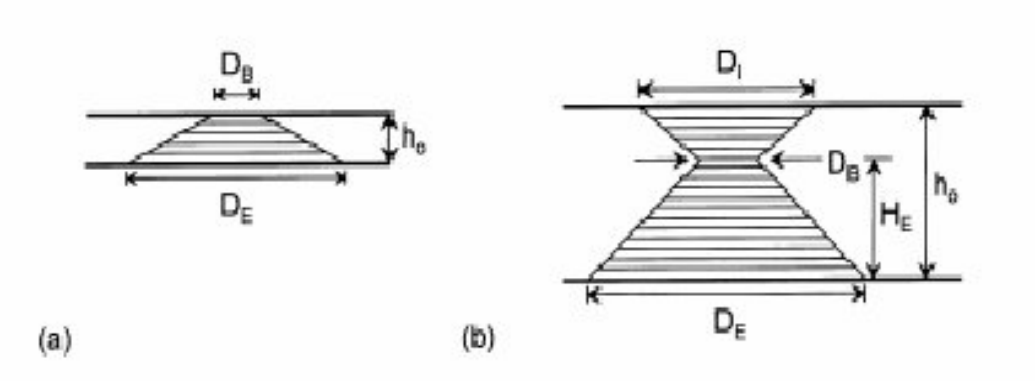


Figure 5.28. The schematic geometry of damage zone of the thin and thick composite (Source: Gellert *et al.* 2000).

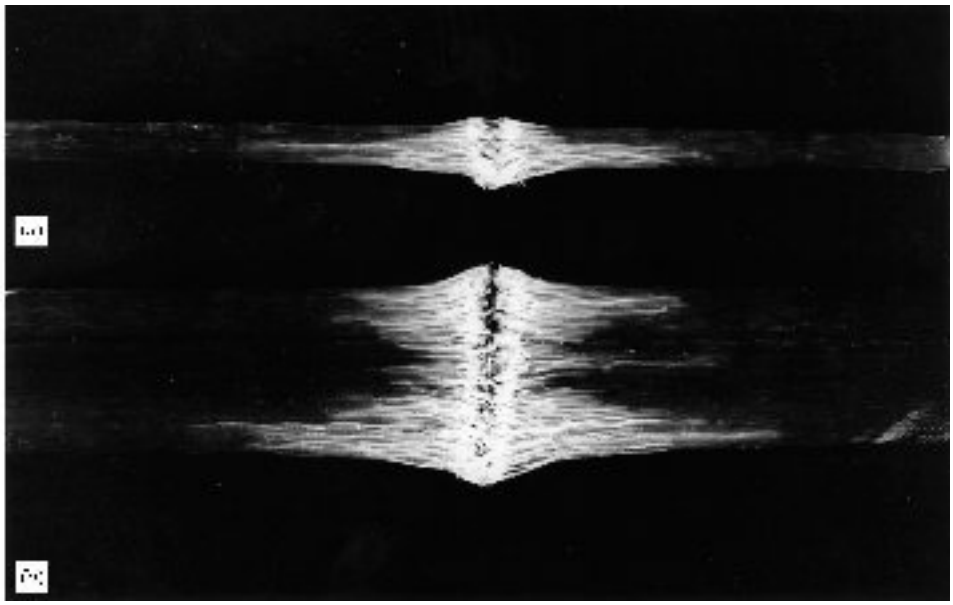

Figure 5.29. The photograph of geometry of damage zone of the thin and thick composite (Source: Gellert *et al.* 2000).

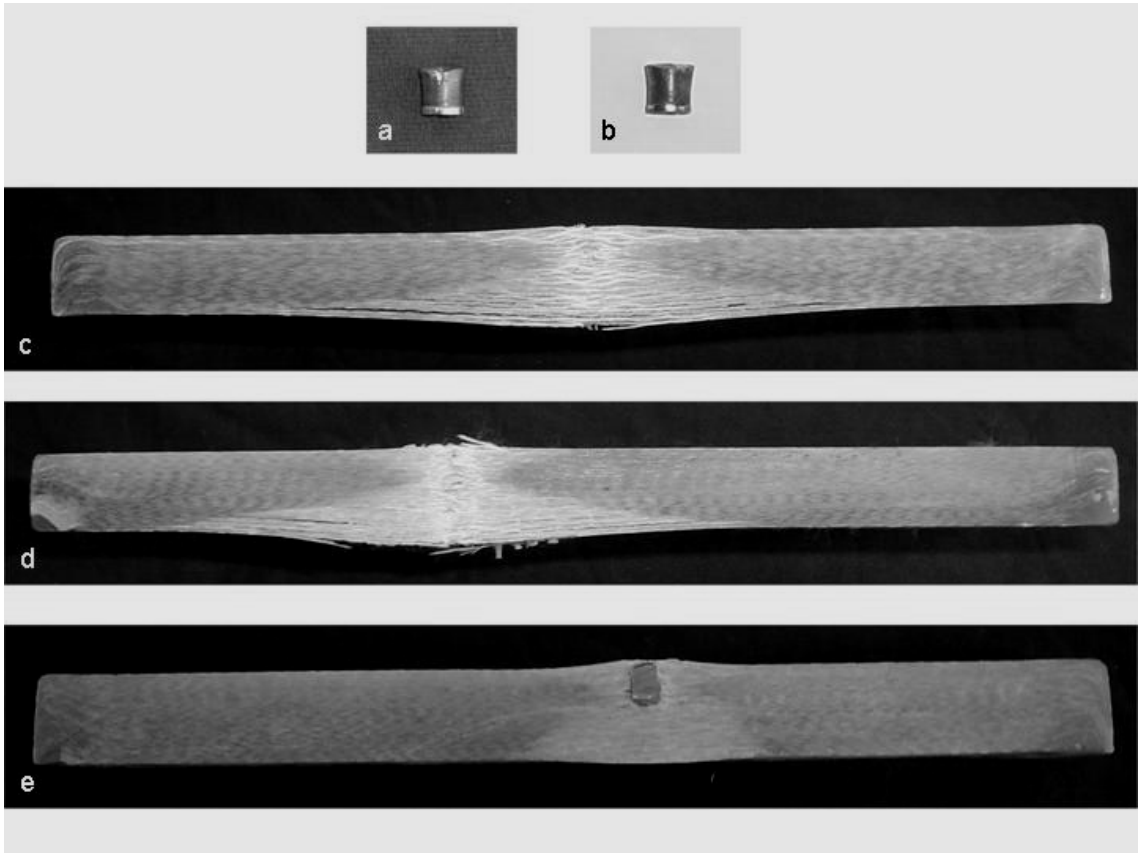


Figure 5.30. The cross section of the polymer composites after ballistic impact and the projectiles. a,b) FSP projectiles c) perforation (panel #3, 2nd shot) d) perforation (panel #9, 1st shot) e) partial penetration (panel #2, 1st shot)

Table 5.7. Ballistic delamination data for the composite panels.

| Number | Projectile type | Velocity (m/s) | Front Damage Diameter (cm) | Back Damage Diameter (cm) | Delamination % (Front Face) | Delamination % (Back Face) |
|---|---|---|---|---|---|---|
| 2-1 | FSP | 435 | 6.35 | 7.8 | 3.51 | 5.30 |
| 2-2 | FSP | 548 | 5.7 | 6.3 | 2.83 | 3.46 |
| 3-1 | FSP | 826 | 5.9 | 13.25 | 3.03 | 15.32 |
| 3-2 | FSP | 1015 | 7.3 | 16.75 | 4.65 | 24.48 |
| 9-1 | FSP | 1001 | 6.6 | 15.35 | 3.80 | 20.56 |
| 9-2 | FSP | 1074 | 6.4 | 14.8 | 3.57 | 19.11 |

## 5.6. Prediction of Values of Composite's Ballistic Behaviour

In Chapter 2, the analytical expressions were given based on the study of Wen (Wen 2000, 2001) to predict the ballistic limit and dept of penetration of the composites subjected to ballistic impact. In this section, the corresponding equations were used to predict the ballistic behavior of the composites with the properties studied within the study.

Figure 5.31 shows the theoretical prediction of the penetration depth vs. initial velocity of the projectile for GRP (E-glass/polyester) laminates impacted by a 7.62 mm diameter conical-nosed AP projectile with a mass of 9.85 g. In the theoretical calculations, the parameters; $\rho_t$= 1879 kg/m$^3$, $\sigma_e$= 532 MPa and $\theta$= 90$^o$, hence $\beta = 2 \sin(\theta/2) = 2 \sin 45 = 1.414$ was taken as described in Equations (2.2) and (2.3). The solid and broken lines in Figure 5.31 are the theoretical predictions by Equations (2.2) and (2.3), respectively.

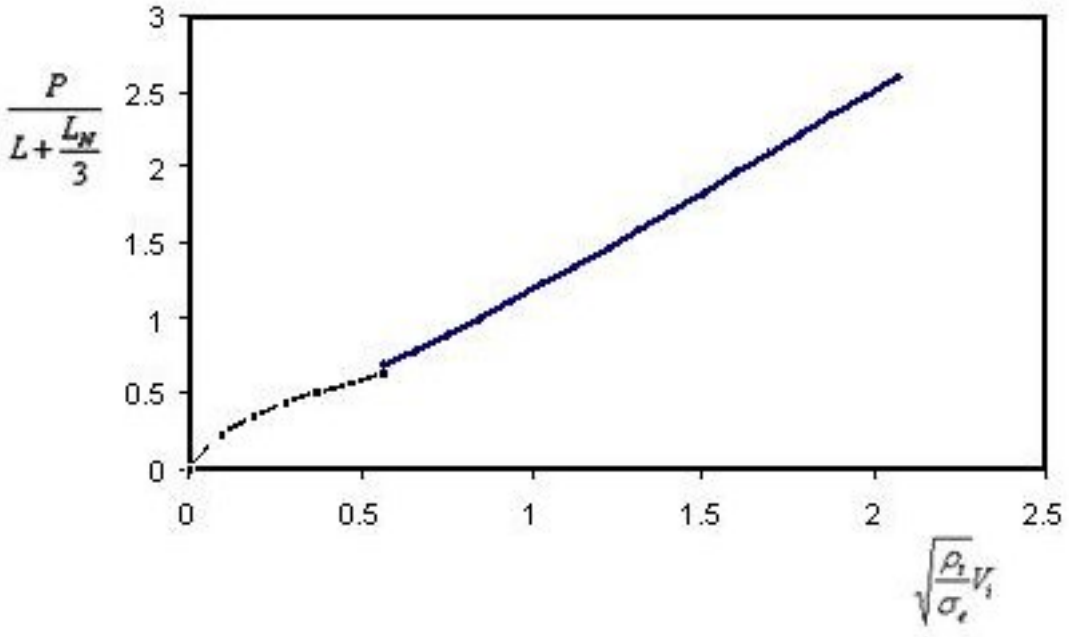


Figure 5.31. The theoretical predictions for the penetration depth within thick GRP (E-glass/polyester) laminates struck normally by a 7.62 mm diameter conical nosed projectile (AP) as a function of normalized initial velocity of the projectile.

Figure 5.32 shows the theoretically predicted ballistic limits for GRP (E-glass/polyester) laminates struck transversely by a 7.62 mm diameter conical-nosed AP

missile with a mass of 9.85 g as a function of composite thickness (T). In the theoretical calculation, $\rho_t$= 1879 kg/m$^3$, $\sigma_e$= 532 MPa and $\theta$= 90$^o$ and hence $\beta$ = 2 sin ($\theta$/2) = 2 sin45 = 1.414 was taken. Also, on the same figure experimental data for the composites impacted by conical-nosed AP projectiles can be seen. For all the experimental velocity values, full penetration of the polymer composite was observed. Therefore, the $V_b$ for those composites are expected to be lower than the data shown on the figure. So, the predicted $V_b$ value are relatively higher than those experimentally measured values.

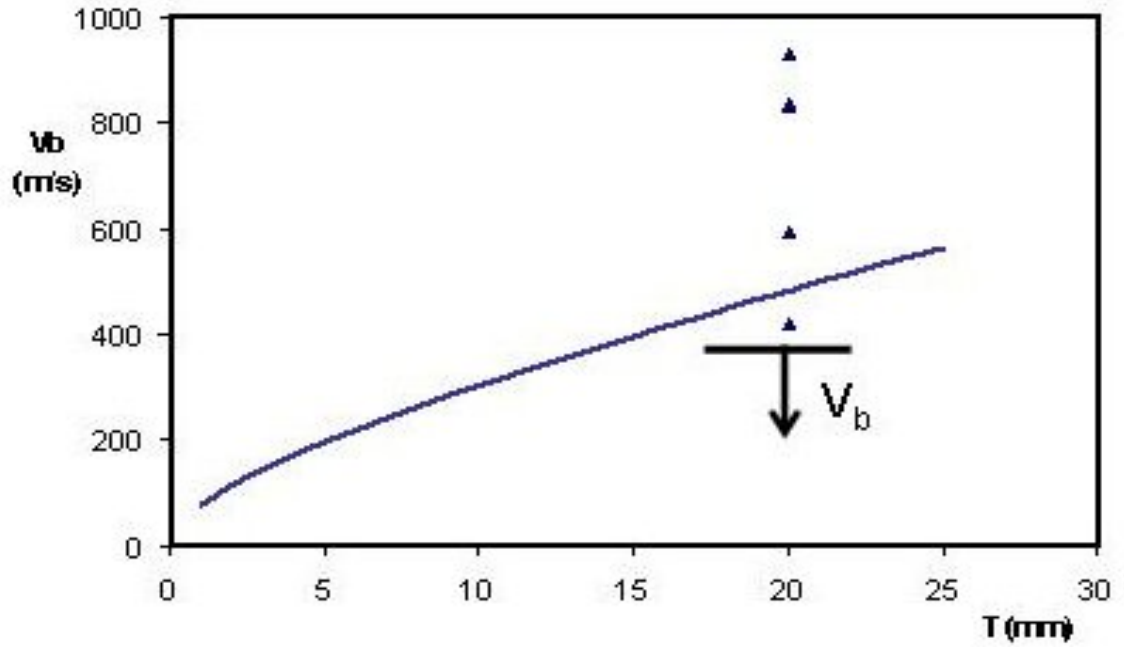


Figure 5.32. Comparison of the theoretical predictions with the experimental data for the ballistic limit of GRP (E-glass/polyester) laminates struck transversely by a 7.62 mm diameter conical-nosed AP missile as a function of panel thickness (T). --:theo., ▲

Figure 5.33 shows the theoretically predicted ballistic limits for GRP (E-glass/polyester) laminates struck transversely by a 7.62 mm diameter flat-faced FSP missile with a mass of 2.85 g as a function of T. In the theoretical calculation, $\rho_t$= 1879 kg/m$^3$, $\sigma_e$= 532 MPa and $\theta$= 180$^o$ and hence $\beta$ = 2 sin ($\theta$/2) = 2 sin90 = 2 was taken. Also, on the same figure experimental data for the composites impacted by FSP projectiles can be seen. For the experimental velocities higher than 831 m/s, full penetration of the polymer composite was occurred. So, the predicted values for this case are also relatively higher than experimentally measured values.

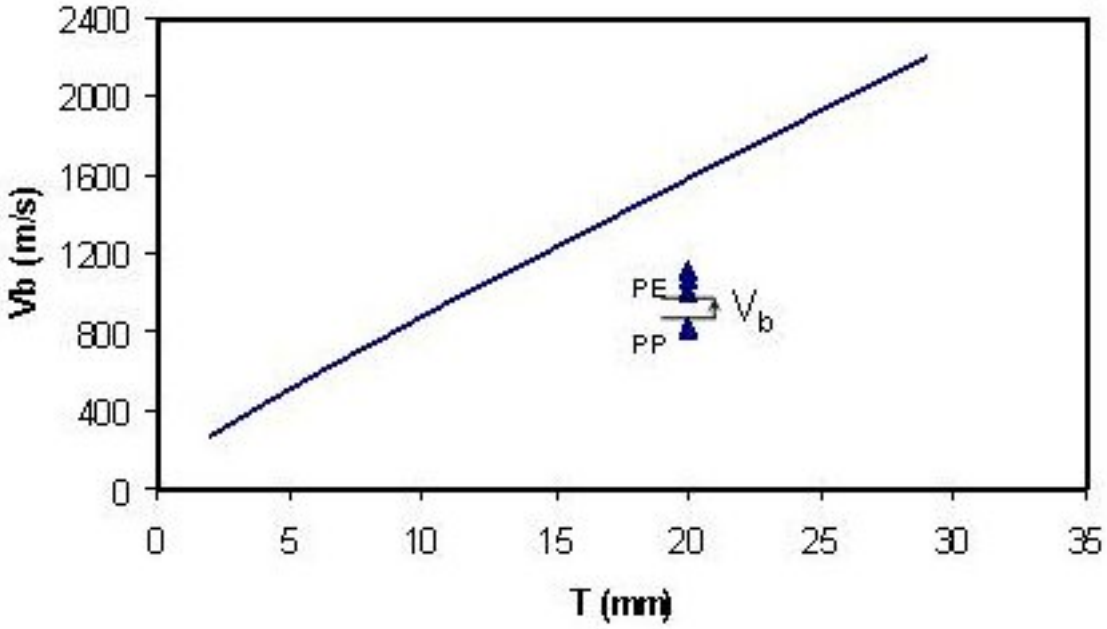


Figure 5.33. Comparison of the theoretical predictions with the experimental data for the ballistic limit of GRP (E-glass/polyester) laminates struck transversely by a 7.62 mm diameter FSP missile. --:theo. ▲ Exp. (PE:perforation, PP: partial penetration

# CHAPTER 6

## CONCLUSIONS

In this study, E-glass fabric/unsaturated polyester composite plates were successfully manufactured by RTM method. Composites were fabricated using $0^o/90^o$ woven fabrics and $0^o/90^o$ biaxial and $0^o/+45^o/-45^o/90^o$ quadraxial non-crimp fabrics The mechanical and ballistic behaviors of those composites were investigated. In addition, ceramic alumina ($Al_2O_3$) tiles or aluminum (Al) plates were incorporated to polymer composites to fabricate sandwich structures for improved ballistic resistance.

From the mechanical test results, it was seen that compressive strength and modulus values of the composites made with woven and non-crimp stitched fibers, in ply lay up direction are higher than the values of compressive strength and modulus in through thickness directions. Besides, the composites laminates made with $0^o/90^o$ woven fabrics exhibited the highest compressive strength values as compared to the composite laminates. Although the composite laminates made with $0^o/+45^o/-45^o/90^o$ quadraxial non-crimp fabrics have the smaller modulus values compared with the laminates includes $0^o/90^o$ woven fabrics; they have nearly same compressive strength with the wovens, also in ply-lay up and in plane directions.

The fracture toughness test results showed that the lowest fracture toughness values in ply-lay up direction were measured from the composite laminates made with $0^o/+45^o/-45^o/90^o$ quadraxial non-crimp fabrics. On the contrary, for in plane direction the highest fracture toughness value belongs to the composite laminates made with $0^o/+45^o/-45^o/90^o$ quadraxial non-crimp fabrics, too.

The composite laminates made with $0^o/90^o$ woven fabrics have the maximum interlaminar shear strength values as compared with the others. For the composites made with multi-axial non-crimp stitched fabrics have nearly same interlaminar shear strength values.

The ballistic test results exhibited that the polymer composites have ballistic resistance against 7.62 mm fragment simulating projectiles (FSP) up to 1001 m/s projectile velocities. However, the composites without any support layer are not sufficient to stop AP projectiles. The sandwich panels containing alumina ceramic tiles

subjected to the ballistic impact by AP and FSP projectiles exhibited only partial penetrations at all the velocities applied within the study (446-1020 m/s with AP and 435-1173 m/s with FSP). It was observed that the alumina tiles that blunt the projectile directly affect the ballistic performance of the composites; however the ballistic test results showed that the aluminum (Al) tiles do not have a significant effect on the ballistic performance of the composite laminates. Cross-sectional analysis of impacted composites revealed that a conical damage zone forms due to ballistic impact within the composites.

The theoretical predictions of the ballistic limit and dept of penetration of the composites subjected to ballistic impact were also investigated in this study. However, the results showed that the theoretical predictions are not in good agreement with the experimental data and the experimental data is in general lower than predicted values.

All the results show that the multilayered composite structures have capacity against the ballistic threats and potential to be used as lightweight armor materials. RTM is suitable process technique to produce composite plates.

# REFERENCES


Advani, S. G., Bruschke, M. V., Parnas, R. S., 1994. "Resin Transfer Molding Flow Phenomena In Polymeric Composites, Flow and Rheology in Polymer Composites Manufacturing", *Elsevier Science*, 1994.

Altan, M. C., Olivero, K. A., Hamidi, Y. K., Aktas, L., 2004. "Effect Of Preform Thickness And Volume Fraction On Injection Pressure And Mechanical Properties Of Resin Transfer Molded Composites", *Journal Of Composite Materials*. Vol. 38, No. 11

Bernetich, K. R., Fink, B.K., Gillespie, J.W., 1998. "Ballistic Testing of Affordable Composite Armour", Baltimore, Maryland, September, pp. 21-21

Bernetich K.R., Fink B.K., Gillespie Jr. J.W. 1998. "Ballistic Testing of Affordable Composite Armor", Proceedings of American Society for Composites, September 1998, Baltimore, Maryland.

Benloulo, I.S.C., Sanchez, V., 1998. "A New Analytical Model to Simulate Impact Onto Ceramic /Composite Armors", *Int.J. Impact Engineering*. Vol.21;6, pp. 461-471.

Bhatnagar, A., Lin, L.C., Lang, D.C., Chang, H.W., 1989. "Comparison of Ballistic Performance of Composites", Proceedings of 34th International Sampe Symposium, (8-11 May 1989).

Brouwer, W.D., van Herpt, E.C.F.C., Labordus, M., 2003. "Vacuum Injection Moulding for Large Structural Applications", *Composites: Part A*. Vol. 34, pp. 551–558

Candan. C., 2005. "Zırh Teknolojilerindeki Gelişmeler " Proceedings of Zırh Teknolojileri Semineri, Ankara, (10-11 Mart 2005), Milli Savunma Bakanlığı Arge ve Teknoloji D. Bşk.lığı.

Choi, J.H., Dharan, C.K.H., 2002. "Mold Filling Time And Void Reduction In Resin Transfer Molding Achieved By Articulated Tooling", *Journal of Composite Materials*. Vol.36, No.19

Cheeseman, B.A. and Bogetti, T.A., 2003. "Ballistic Impact into Fabric and Compliant Composite Laminates", *Composite Structures*, Vol. 61, pp.161-173.

DEF STAN 05-101, (Ministry of Defence, Defence Standard), 2005, "Proof of Ordnance, Munitions, Armour and Explosives", Issue 1, Part 2, 20 May 2005

DEF STAN 95-24/3, (Ministry of Defence, Defence Standard), 2004, "Armour Plate Steel (3-160 mm)" Issue 3, 23 January 2004.

DEF STAN 95-22, (Ministry of Defence, Defence Standard), 2004, "Aluminium Alloy Armor Plate (Heat Treatable 1-120 mm)", Issue 4, 3 September 2004.

DEF STAN 95-25, (Ministry of Defence, Defence Standard), 2004, "Armor Quality Steel Castings", Issue 2, 3 September 2004.

DEF STAN 95-23, (Ministry of Defence, Defence Standard), 2004, "Ferrous Armor Quality Extrusion & Forgings", Issue 2, 3 September 2004.

DEF STAN 95-23, (Ministry of Defence, Defence Standard), 2004, "Armor Aluminium Homogenous Alloy, Heat Treatable, Extrusion & Forgings (6 mm thick and over)" Issue 3, 3 September 2004.

Devillard, M., Hsiao, K., Gokce, A., Advani, S.G., 2003. "On-Line Characterization Of Bulk Permeability And Race-Tracking During The Filling Stage In Resin Transfer Molding Process", *Journal of Composite Materials*. Vol.37, No.17

Elperin, T., Ben-Dor, G., Dubinsky, A., Frage, N., 2000a, "Optimization of two Component Ceramic Armor for a Given Impact Velocity", *Theoretical and Applied Fracture Mechanics*, Vol.33, pp.185-190.

Elperin, T., Ben-Dor, G., Dubinsky, A., 2000b, "The Optimum Arrangement of the Plates in a Multi-Layered Shield"

Ferret, B., Anduze , M., Nardari , C., 1998. "Metal Inserts in Structural Composite Materials Manufactured by RTM", *Composites Part A.* Vol.29A, pp.693-700

Fındık, F., Tarim, N., Uzun, H., 2002. "Ballistic Performance of Composite Structures", *Composite Structures*, Vol.56, pp.13-20.

Fong, L., Advani, S.G., 1998. "Resin Transfer Molding", *Handbook of Composites*, (Chapman&Hall, London), pp. 434-452.

Gama, B.A,., Bogetti, T.A., Fink, B.K., Mahfuz, H., Gillespie, J. W., 1999. "Modeling and Simulation of Dynamic Behaviour of EPDM Rubber under Stress Wave Loading", Proceedings of Mathematics and Computers in Mechanical Engineering '99, (July 25-29), Florida Keys, (CD ROM)

Gama, B.A., Bogetti, T.A., Fink, B.K., Yu, C., Claar, D.T., Eifert, H.H., Gillespie, Jr. J.W., 2001. "Aluminum foam integral armor: a new dimension in armor design", *Composite Structures,* Vol.52, pp.381-395

Gellert, E.P., Cimpoeru, S.J., Woodward, R.L., 2000. "A study of the Effect of Target Thickness on the Ballistic Perforation of Glass-fibre-reinforced Plastic Composites", *Int. J. of Impact Engineering*, Vol.24, pp.445-456.

Hammami, A., Gauvin, R., Trochu , F., Touret, O., Ferlan, P., "Analysis of the Edge Effect on Flow Patterns in Liquid Composites Molding", *Applied Composite Materials.*Vol. 5, pp.161-173

Hammami, A., Gauvin, R., Trochu, F., 1998. "Modelling the Edge Effect in Liguid Composites Molding", *Composites Part A.* Vol. 29A, pp. 603-609.

Hillermeier, R.W., Seferis, J.C., 2001. "Interlayer Toughening of Resin Transfer Molding Composites", *Composites: Part A.* Vol.32, pp.721-729.

Hsiao, K., Advani, S. G., 2004. "Flow Sensing And Control Strategies To Address Race-Tracking Disturbances In Resin Transfer Molding. Part I: Design And Algorithm Development", *Composites: Part A*

Hull, D., 1995. "An Introduction to Composite Materials", (Cambridge Solid State Science Series), pp. 31-47.

Hetherington, J.G., 1992 "The Optimization of Two Component Composite Armours", *Int. J. of Impact Engineering*. Vol.12 No:3, pp. 409-414.

High Performance Composites, 2005. "Ballistic Protection", (Ray Publishing Inc.), pp.26-31

High Performance Composites, 2003. "Manufacturing Control Software", pp.18-22

Hogg, P. J., 2003. "Composites for Ballistic Applications", Proceedings of Composite Processing 2003, CPA, Bromgrove, U.K.

Horsfall I, Austin S.J, Bishop W. 2000. "Structural ballistic armour for transport aircraft", *Materials and Design*, Vol. 21, p.19-25

Jang, B. Z., 1994. "Advanced Polymer Composites; Principles and Applications", ASM International, pp.1-21.

Johnson, C.F., 1987. "Resin Transfer Molding", *Engineered Materials Handbook*, Composites, ASM International, Volume 1, pp.564-568.

Kim, P. J., Lee, D.G., 2002, "Surface Quality and Shrinkage of the Composite Bus Housing Panel Manufactured By RTM", *Composite Structures* . Vol.57, pp. 211-220.

Kang, M. K., Jung, J. J., Lee , W., 2000. "Analysis Of Resin Transfer Moulding Process With Controlled Multiple Gates Resin Injection", *Composites: Part A*. Vol. 31, pp. 407–422

Larsson F, Svensson L. 2002. "Carbon, polyethylene and PBO hybrid fibre composites for structural lightweight armour", *Composites: Part A*, Vol. 33, p.221-231

Lee, N.J., Lee , H., J., Lee, K.J., Nam, J.D., 2002. "Effects of Surface Modification on the Resin Transfer Moulding (RTM) of Glass fibre/unsaturated Polyester Composites", *Composites Science and Technology*. Vol. 62, pp. 9–16

Lee, M., Yoo, Y.H., 2001. "Analysis of Ceramic/Metal Armour Systems", *International Journal of Impact Engineering*. Vol. 25, pp. 819–829

Mahdi S., Gama B.A., Yarlagadda S., Gillespie Jr. J.W. 2003 "Effect of the manufacturing process on the interfacial properties and structural performance of multi-functional composite structures", *Composites: Part A*; Vol.34, pp.635-647

Meyers, M.A., 1994. *Dynamic Behavior of Materials*, (John Wiley Inc.) p.597

Mccafery, T. R., Zguris, Z.Z., Durant, Y. G., 2003. "Low Cost Mold Development for Prototype Parts Produced by Vacuum Assisted Resin Transfer Molding (VARTM)", *Journal Of Composite Materials.* Vol 37, No:10

Monib, A. M., 1998. "Damage Tolerance of Thick-Section Composites Subjected To Ballistic Impact", *CCM Report 99-08, Center for Composite Materials, University of Delaware*.

Morye S.S., Hine P.J., Duckett R.A., Carr D.J., Ward I.M. 2000. "Modelling of the energy absorption by polymer composites upon ballistic impact", *Composites Science and Technology*, Vol.60, p.2631-2642

Naik, N. K., Shrirao, P., 2004. "Composite Structures under Ballistic Impact", *Composite Structures*, Vol.66, pp.579-590.

Navarro, C., Martinez, M.A., Cotes, R., Sanchez-Galvez, V., 1993. "Some Observations on the Normal Impact on Ceramic Faced Armours Backed by Composite Plates", *Int. J. Impact Eng.* Vol.13, No.1, pp 145-156

Navarro, C., Zaera. R., Saez, S., Castellanos. J.L., 2000. "Modelling of the Adhesive layer in mixed Ceramic/Metal Armours Subjected to Impact", *Composites: Part A*, Vol. 31, pp.823-833.

NIJ Standard-01.01.04, 2001. National Institute of Justice, "Ballistic Resistance of Personal Armor"

Potter, K., "Resin Transfer Molding", Chapman & Hall, London, 1997

Ranganath, S., Subrahmanyam, J., 1998. "Ballistic Testing and Evaluation of Ceramic Composites", Defence Metallurgical Research Laboratory, Kanchanbagh, Hyderabad, India.

Rouisona , D., Sainb, M., Couturiera, M., 2004. "Resin Transfer Molding Of Natural Fiber Reinforced Composites: Cure Simulation", *Composites Science and Technology*. Vol. 64, pp. 629–644

Ruiz, E., Trochu, F., 2005. "Numerical Analysis Of Cure Temperature And Internal Stresses In Thin And Thick RTM Parts", *Composites: Part A*. Vol. 36, pp. 806–826

Sadanandan, S., Hetherington, J.G., 1997. "Characterization of Ceramic/Steel and Ceramic/Aluminium Armors Subjected to Oblique Impact", *Int. J. Impact Engineering*. Vol.19, No.9-10, pp. 811-819

Schmachtenberg, E., Schulte zur Heide, J., Töpker, J., 2005. "Application of Ultrasonics for the Process Control of Resin Transfer Moulding (RTM)", *Polymer Testing*. Vol. 24, pp. 330–338

Sebe, G., Cetın, N. S., Hill, C. S., Hughes, M., 2000. "RTM Hemp Fibre-Reinforced Polyester Composites", *Applied Composite Materials*. Vol. **7,** pp. 341–349

Standard test method for flexural properties of unreinforced and reinforced plastics and electrical insulating materials. Annual book of ASTM standards, Vol. 08.03, 1986, 290-298.

Standard test method for apparent interlaminar shear strength of parallel fiber composites by short-beam method. Annual book of ASTM standards, Vol. 08.02, 1989

Standard method for compressive properties of rigid plastics. Annual book of ASTM standards, Vol 14.02, 1996, 76-82.

Strong, A. B., 1989. "Fundamentals of Composites Manufacturing", *Society of Manufacturing Engineers.*,pp. 134-137.

Tanoğlu, M., McKnight, S.H., Palmese, G.R., Gillespie, Jr. J.W., 2001. "Effects of Glass Fiber Sizings on the Strength and Energy Absorption of the Fiber/Matrix interphase under high Loading Rates", *Material Science and Engineering*, Vol.61, pp.205-220

Tanoğlu M., Seyhan A.T., 2002. "Investigating the effects of a polyester preforming binder on the mechanical and ballistic performance of E-glass fiber reinforced polyester composites", *Int. J. of Adhesion and Adhesives*; 23:1-8.

Ulven C, Vaidya U.K., Hosur M.V. 2003. "Effect of projectile shape during ballistic perforation of VARTM carbon/epoxy composite panels", *Composite Structures*, Vol. 61, p.26-31

Vaidya, U. K., Abraham, A., Bhide, S., 2001. "Affordable Processing of Thick Section and Integral Multi-Functional Composites", *Composites: Part A.* Vol.32, pp. 1133-1142.

Wang, B., Lu, G., 1996. "On The Optimisation of Two-Component Plates against Ballistic Impact", *Journal of Materials Processing Technology,* Vol. 57, pp.141-145.

Wang B., Chou S.M.,1997."The Behaviour Of Laminated Composite Plates As Armour". *Journal of Materials Processing Tecnology*. Vol. 68, pp.279-287

Wang Y., 2002. "Mechanical Properties of Stitched Multiaxial Fabric Reinforced Composites from Mannual Layup Process". *Applied Composite Materials,* Vol. 9, pp.81-97.

Warda I.M., Moryea S.S., Hinea P.J., Ducketta R.A., Carrb D.J., 1999. "A Comparison of the Properties of Hot Compacted Gel-Spun Polyethylene Fibre Composites with Conventional Gel-Spun Polyethylene Fibre Composites" *Composites: Part A*, Vol.30, pp.649–660.

Warrior, N.A., Turner, T.A., Robitaille, F., Rudd, C.D., 2003. "Effect of Resin Properties and Processing Parameters on Crash Energy Absorbing Composite Structures Made by RTM", *Composites: Part A*. Vol. 34, pp. 543–550

Wen, H.M., 2001. "Penetration and Perforation of Thick FRP Laminates", *Composites Science and Technology*, Vol.61, pp. 1136-1172.

Wen, H.M., 2000. "Predicting the Penetration and Perforation of FRP Laminates Struck Normally by Projectiles with Different Nose Shapes", *Composite Structures,* Vol.49, pp. 321-329.

WEB_1, www.armylab.com

WEB_2, 2005. www.compositesworld.com

WEB_3, 2004. www.metyx.com

Zaera, R., Galvez, V., 1998. "Analytical Modelling of Normal and Oblique Ballistic Impact on Ceramic/Metal Lightweight Armour", *Int. J. Impact Engineering*, Vol. 21, No. 3, pp.133-148.